JCB Journal of Cell Biology

ARTICLE

SM protein Sly1 and a SNARE Habc domain promote membrane fusion through multiple mechanisms

Mengtong Duan[1], Guanbin Gao[2], Ariel Lin[1], Emma J. Mackey[1], David K. Banfield[2], and Alexey J. Merz[1]

SM proteins including Sly1 are essential cofactors of SNARE-mediated membrane fusion. Using SNARE and Sly1 mutants and chemically defined in vitro assays, we separate and assess proposed mechanisms through which Sly1 augments fusion: (i) opening the closed conformation of the Qa-SNARE Sed5; (ii) close-range tethering of vesicles to target organelles, mediated by the Sly1-specific regulatory loop; and (iii) nucleation of productive trans-SNARE complexes. We show that all three mechanisms are important and operate in parallel, and that close-range tethering promotes trans-complex assembly when *cis*-SNARE assembly is a competing process. Further, we demonstrate that the autoinhibitory N-terminal Habc domain of Sed5 has at least two positive activities: it is needed for correct Sed5 localization, and it directly promotes Sly1-dependent fusion. "Split Sed5," with Habc presented solely as a soluble fragment, can function both in vitro and in vivo. Habc appears to facilitate events leading to lipid mixing rather than promoting opening or stability of the fusion pore.

Introduction

SNARE-mediated membrane fusion is central to secretory cargo transport, exocytosis, and organelle biogenesis and homeostasis (Jahn and Fasshauer, 2012; Ungar and Hughson, 2003). Fusion is preceded by tethering, mediated by a diverse group of proteins, and usually controlled by small G proteins of the Rab, Arf, or Rho families (Angers and Merz, 2011; Bombardier and Munson, 2015; Pfeffer, 2017; Stenmark, 2012). Tethering is followed by docking: the assembly of a parallel, tetrahelical trans-SNARE complex ("SNAREpin") that bridges the two membranes (Hanson et al., 1997; Nichols et al., 1997; Sutton et al., 1998; Weber et al., 1998). "Zippering" of the incipient trans-SNARE complex does the mechanical work of driving the membranes together to initiate fusion (Zorman et al., 2014). The trans-SNARE complex contains four α-helices, one from each of the four SNARE subfamilies: R, Qa, Qb, and Qc (Fasshauer et al., 1998). R-SNAREs often correspond to vesicle or v-SNAREs, while Qa-SNAREs (also called syntaxins) typically correspond to the target membrane or t-SNAREs. The Qa-SNAREs have in common an N-terminal regulatory "Habc" domain that folds into a trihelical bundle. In some, but not all cases, the Habc domain can fold back onto the catalytic SNARE domain to form an autoinhibited "closed" conformation (Demircioglu et al., 2014; Dulubova et al., 1999, 2001; Fernandez et al., 1998; Kosodo et al., 1998; Misura et al., 2000; Struthers et al., 2009).

In addition to SNAREs and tethering factors, proteins of the Sec1/mammalian Unc-18 (SM) family have indispensable roles in SNARE-mediated fusion (Carr and Rizo, 2010; Rizo and Südhof, 2012; Stanton and Hughson, 2023; Südhof and Rothman, 2009). SMs were first identified through genetic screens: *Drosophila* Vps33a (Carnation; Patterson, 1932); *Saccharomyces cerevisiae* Sec1; and UNC-18 in *Caenorhabditis elegans*, later identified as Munc18 or nSec1 in mammals (Brenner, 1974; Hata et al., 1993; Novick and Schekman, 1979; Pevsner et al., 1994). Despite early identification, strong mutant phenotypes, and major efforts by many groups, the general mechanisms of SM function are only recently emerging. All SMs exhibit strong evolutionary and structural homology but they interact with cognate SNARE proteins in different ways. For example, yeast Sly1, yeast Vps45, and Munc18-1 all interact with short N-peptides at the amino termini of their cognate Qa-SNARE proteins (Bracher and Weissenhorn, 2002; Carpp et al., 2006; Dulubova et al., 2002; Furgason et al., 2009; Grabowski and Gallwitz, 1997; Hata et al., 1993; Yamaguchi et al., 2002). In contrast, Qa-SNARE N-peptide interactions do not occur with human or yeast Vps33, or with yeast Sec1 (Baker et al., 2015; Dulubova et al., 2001; Lobingier and Merz, 2012; Togneri et al., 2006). We have called SM proteins that interact with Qa-SNARE N-peptides Class I and those that do not Class II (Lobingier and Merz, 2012).

Early structural and biochemical studies revealed that Munc18-1 clamps the Qa-SNARE Syntaxin-1A in its closed

[1]Department of Biochemistry, University of Washington, Seattle, WA, USA; [2]The Division of Life Science, The Hong Kong University of Science and Technology, Kowloon, Hong Kong.

Correspondence to Alexey J. Merz: merza@uw.edu.

conformation, suggesting an inhibitory role for the SM. (Dulubova et al., 1999; Misura et al., 2000; Yang et al., 2000). However, the emerging consensus is that the core and evolutionarily conserved role of SM proteins is positive rather than inhibitory. Specifically, SM proteins are hypothesized to nucleate and stabilize fusion-competent trans-SNARE complexes (Carr and Rizo, 2010; Südhof and Rothman, 2009; Toonen and Verhage, 2003; Yoon and Munson, 2018). A breakthrough was achieved in 2015 with two structures of yeast Vps33: one bound to a Qa-SNARE domain and another bound to an R-SNARE domain (Baker et al., 2015). When superimposed, the structures implied that Vps33 templates initial assembly of the trans-SNARE complex, allowing the trans-complex to transit into a metastable, half-zipped intermediate referred to as the "template complex." Single-molecule force spectroscopy experiments strongly supported this interpretation (Jiao et al., 2018; Ma et al., 2015). It remains unclear to what extent SMs promote SNARE-mediated fusion through additional general or pathway-specific mechanisms.

We have turned our attention to Sly1, the ER–Golgi SM. Sly1 has been proposed to promote fusion through several different mechanisms. First, meticulous solution biochemistry demonstrated that Sly1 can open the inactive closed conformation of the Qa-SNARE, Sed5. This in turn allows Sed5 to more readily complex with Qb, Qc, and R-SNAREs (Bos1, Bet1, and Sec22 [Demircioglu et al., 2014; Kosodo et al., 1998]). A limitation of this work is that the SNAREs used were soluble fragments. The roles of Sed5 inhibition and opening were not tested in membrane fusion experiments. Second, we demonstrated that Sly1 binding to quaternary SNARE complexes in solution slows the kinetics of ATP-dependent disassembly by Sec17 and Sec18 (in mammals, α-SNAP and NSF). Consistent with these findings, in vivo genetic tests revealed that Sec17 overproduction is tolerated in a wild-type genetic background but lethal when Sly1 function is partially compromised (Lobingier et al., 2014). Third, on the basis of structural homology to Vps33, Baker et al. (2015) proposed that Sly1 can template Qa- and R-SNARE trans-complex formation. Fourth, experiments in a companion manuscript (Duan et al., 2024) demonstrate that Sly1 promotes close-range vesicle tethering through an amphipathic helix, α21, that directly captures the incoming vesicle membrane and regulates R-SNARE assembly.

All of these mechanisms could promote fusion but no study to date has attempted to assess their relative contributions within a cohesive experimental framework. Here, we begin that effort, combining in vivo genetic tests with a chemically defined in vitro reconstitution of fusion on the ER-Golgi anterograde pathway. Focusing on Sly1 interactions with the Qa-SNARE Sed5, we demonstrated that multiple mechanisms do indeed contribute to Sly1's fusion-promoting activity. Additionally, our results prove that the regulatory Habc domain of the Qa-SNARE Sed5 augments Sly1-stimulated fusion rather than being solely autoinhibitory.

Results

Sed5 N-peptide is essential for viability and efficient fusion

The Qa-SNARE Sed5 has five domains: an N-peptide of 21 residues that binds tightly to Sly1; a trihelical Habc domain that is autoinhibitory; a flexible linker region; the Qa-SNARE domain; and the C-terminal transmembrane helix (Fig. 1 A). In a previous study, missense mutations that reduced the affinity of Sly1 for the N-peptides of its client Qa-SNAREs (Sed5 and Ufe1) resulted in minimal defects in assays for viability, secretion, and Sly1 localization. This was said to indicate the functional "irrelevance" of Sly1–Sed5 interactions (Peng and Gallwitz, 2004). However, more recent experiments indicate that Sly1 binding to the Sed5 N-peptide is essential for viability (Gao and Banfield, 2020), while in mammalian cells, overexpression of a Sly1 cognate N-peptide or the Sly1 N-peptide binding domain shatters the Golgi (Dulubova et al., 2003; Yamaguchi et al., 2002). To further scrutinize whether the Sed5 N-peptide is functionally important in budding yeast, we engineered an allele, *sed5ΔN*, that encodes a Sed5 variant lacking its N-peptide (as defined by crystal structure PDB 1MQS; (Bracher and Weissenhorn, 2002); Fig. 1 A). In a genetic background expressing wild type *SLY1*, *sed5ΔN* is recessive lethal (Fig. 1 B and Fig. S1). Thus, the Sed5 N-peptide is essential for viability. These results are further buttressed by experiments showing that *sed5*(DTFV), a quadruple missense allele that impairs Sly1 binding to the Sed5 N-peptide, is also recessive lethal (Gao and Banfield, 2020).

To test whether the Sed5 N-peptide has a direct role in Sly1-dependent fusion, we used a chemically defined assay of fusion driven by ER-Golgi SNAREs (Duan et al., 2024; Zucchi and Zick, 2011). Briefly, we prepared reconstituted proteoliposomes (RPLs) bearing ER-Golgi SNAREs, with two orthogonal FRET reporter pairs (Fig. 1, C and D). These simultaneously monitor lipid and content mixing in a single 20 µl reaction. We mainly present content mixing data (the reaction endpoint). Fusion requires the presence of Sly1 and also depends on 3% polyethylene glycol, a molecular crowding agent that mimics the action of tethering factors (Duan et al., 2024; Furukawa and Mima, 2014; Lentz, 2007; Mitchison, 2019; Yu et al., 2015). Sly1-mediated fusion is further stimulated by the universal SNARE disassembly chaperones Sec17 and Sec18 (in mammals, α-SNAP and NSF).

To test the function of the N-peptide, we prepared RPLs bearing either wild-type Sed5 or Sed5ΔN (lacking the first 21 aminoacyl residues), and the Qb- and Qc-SNAREs, Bos1 and Bet1. These Q-SNARE RPLs were assayed for their ability to fuse with RPLs bearing the R-SNARE Sec22. In reactions containing Sec17, Sec18, and Mg^{2+}·ATP, fusion was rapid and efficient when both 3% PEG and Sly1 were present. However, the rate and extent of fusion markedly decreased when RPLs bearing Sed5ΔN were tested. Moreover, high concentrations of Sly1 were required to stimulate the fusion of Sed5ΔN RPLs. With wild type Sed5, near-maximal fusion was observed at 100 nM Sly1, while with Sed5ΔN, the rate and extent of fusion were much lower, even at 1,600 nM Sly1 (compare Fig. 1, E and F). When PEG (which promotes vesicle tethering) was omitted (Fig. 1, G and H), fusion with Sed5ΔN was abolished, even with 1,600 nM Sly1. We concluded that the Sed5 N-peptide strongly promotes Sly1-dependent fusion, both in vivo and in vitro.

Sly1 hyperactivity suppresses *sed5ΔN* lethality and restores fusion

The hyperactive *SLY1-20* allele was initially identified as a dominant, single-copy suppressor of loss of Ypt1, the yeast Rab1

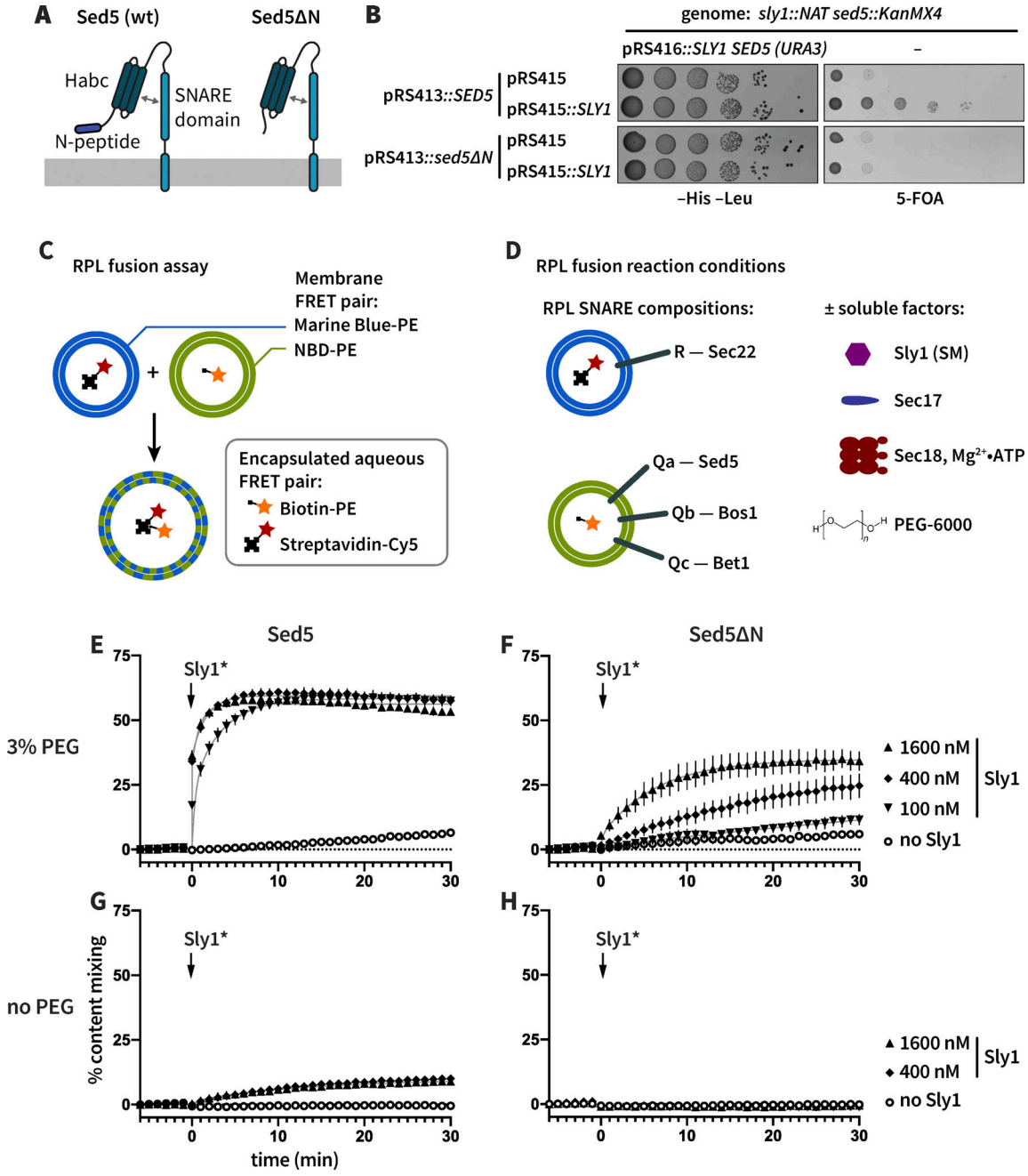

Figure 1. **The N-peptide of Sed5 is essential for viability and efficient fusion. (A)** Diagram showing the constructs tested. Sed5-ΔN lacks the first 21 aminoacyl residues. **(B)** Viability tests. The *sed5-ΔN* allele was tested using *sed5Δ sly1Δ* double knockout cells that carry intact copies of both *SED5* and *SLY1* on a single counter-selectable plasmid. Forced ejection of the *SED5 SLY1* plasmid by plating onto 5-fluoroorotic acid (5-FOA) resulted in lethality unless both *SED5* and *SLY1* were supplied in trans. Additional controls are presented in Fig. S1. **(C)** Reporter systems for lipid and content mixing. RPLs (reconstituted proteoliposomes) are prepared with encapsulated content mixing FRET pair, and with the membranes doped with an orthogonal FRET pair. **(D)** SNARE topology and soluble factors that were added in these experiments. **(E–H)** Reactions were set up with RPLs, Sec17, Sec18, Mg^{2+}·ATP, and 3% (E and F) or 0% (G and H) PEG. Q-SNARE liposomes bore either wild-type Sed5 (E and G) or Sed5ΔN (F and H). The reactions were incubated for 5 min and fusion was initiated by adding Sly1 as indicated at t = 0. Points show mean ± SEM of at least three independent experiments. Gray lines show least-squares fit of a second-order kinetic function.

homolog (Dascher et al., 1991; Ossig et al., 1991). Single-copy *SLY1-20* was subsequently found to suppress deficiencies of a wide variety of proteins that mediate intra-Golgi, ER-Golgi, and Golgi-ER vesicle docking and fusion. In the companion paper (Duan et al., 2024), we show that the mechanism of Sly1-20 hyperactivity involves both the release of Sly1 autoinhibition and coupled activation of a vesicle tethering activity within the Sly1 autoinhibitory domain. *SLY1-20* was able to suppress the lethal phenotype of *sed5ΔN* (Fig. 2 A), but only when *SLY1-20* was provided on a 2-μm plasmid with an average copy number of 15

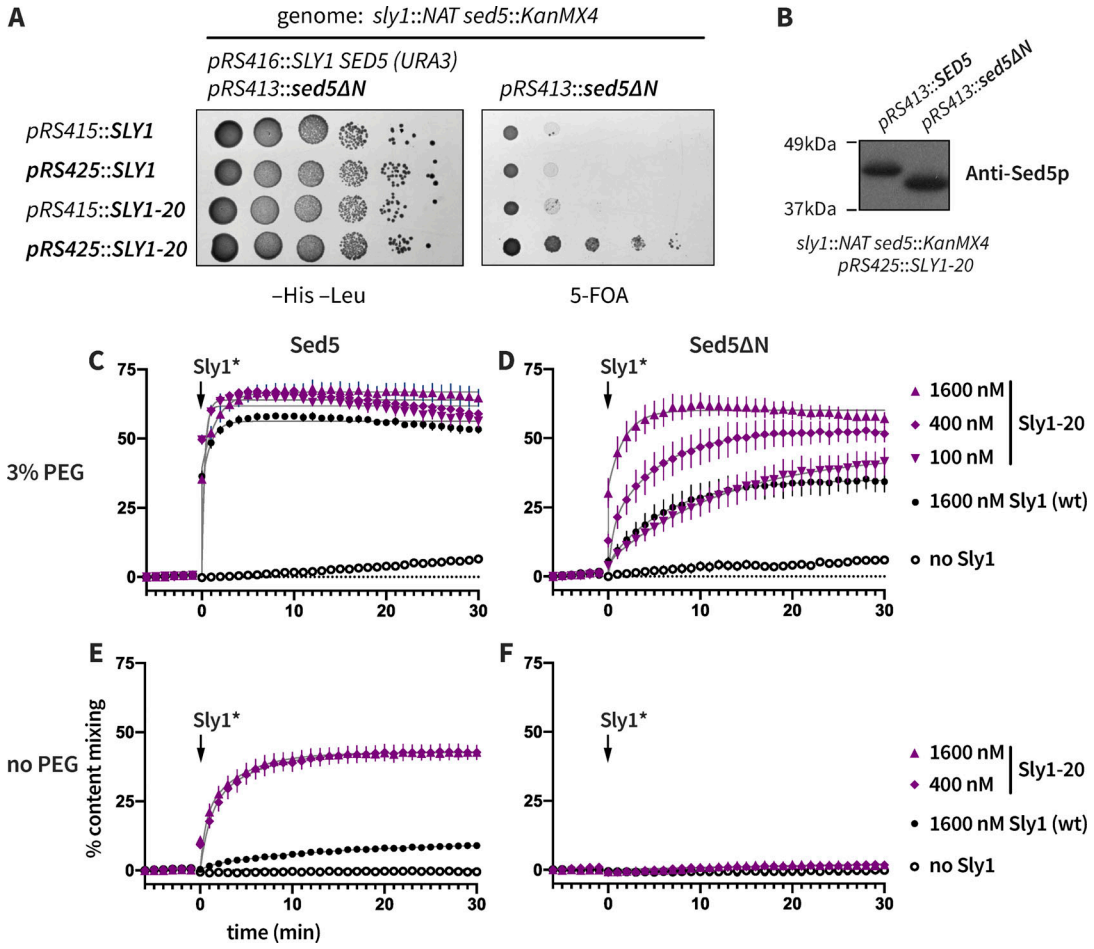

Figure 2. **Sly1-20 can bypass either loss of Sed5 N-peptide or deficient tethering, but not both. (A)** In vivo lethality of *sed5ΔN* is suppressed by *SLY1-20* expressed from a multiple-copy plasmid (pRS425) but not from a single-copy plasmid (pRS415). Growth assays were performed as in Fig. 1; a more extensive set of controls is presented in Fig. S1. **(B)** In the presence of high-copy Sly1-20, the abundance of Sed5ΔN is similar to that of wild-type Sed5. Cell extracts were prepared and analyzed by immunoblotting with anti-Sed5 antiserum. **(C–F)** Reactions were set up with RPLs, Sec17, Sec18, Mg^{2+}-ATP, and 3% (C and D) or 0% (E and F) PEG. Q-SNARE liposomes bore either wild-type Sed5 (C and E) or Sed5ΔN (D and F). The reactions were incubated for 5 min and fusion was initiated by adding Sly1 or Sly1-20 at t = 0. Points show mean ± SEM of at least three independent experiments. Gray lines show least-squares fits of a second-order kinetic function. Source data are available for this figure: SourceData F2.

per cell (Karim et al., 2013). Single-copy *SLY1-20*, or high-copy wild-type *SLY1*, were unable to rescue the growth of *sed5ΔN* mutant cells. Thus *sed5ΔN* is more deleterious than the already-lethal *ypt1-3* (Rab1-deficient) or *uso1Δ* (p115/Uso1 tethering factor-deficient) alleles, both of which are suppressed by single-copy *SLY1-20*. The survival of *sed5ΔN* cells containing high-copy *SLY1-20* allowed us to verify that Sed5ΔN is present at normal abundance and migrates as expected by SDS-PAGE and immunoblot (Fig. 2 B).

Genetic suppression can occur through direct or indirect mechanisms. We used the RPL system to test whether suppression of *sed5ΔN* by *SLY1-20* is direct or indirect. In the presence of PEG, Sly1-20 at 1,600 nM was able to drive fusion of Sed5ΔN RPLs to nearly the rates and extents seen with wild-type Sed5 RPLs and wild type Sly1 at 100 nM (compare Fig. 2, C and D). However, in the absence of PEG (that is, under tethering-deficient conditions), Sly1-20 was unable to drive the fusion of RPLs bearing Sed5ΔN, even at the highest concentrations tested (Fig. 2, E and F). Taken together, these fusion experiments closely mirror the in vivo matrix of genetic interactions among *SED5* and *SLY1* alleles. When wild-type Sly1 is present, fusion is severely attenuated if the Sed5 N-peptide is deleted, but at high concentrations, Sly1-20 rescues Sed5ΔN. With wild-type Sed5, Sly1-20 at moderate concentrations compensates for tethering deficiencies either in vitro (0% PEG) or in vivo (e.g., *ypt1* or *uso1* deficiency). However, in both vesicle tethering assays (Duan et al., 2024) and fusion experiments, hyperactive Sly1-20 cannot compensate for the simultaneous loss of both the Sed5 N-peptide and an extrinsic tethering activity.

Sly1 can stimulate fusion independently of Sed5 opening

Sly1 opens closed Sed5 to promote the assembly of SNARE core complexes (Demircioglu et al., 2014). However, we hypothesized that Sed5 opening is only one of the multiple mechanisms through which Sly1 stimulates fusion. To test this idea, we prepared RPLs bearing two different Sed5 mutants that cannot adopt a closed conformation (Fig. 3 A). Sed5ΔHabc lacks the autoinhibitory Habc domain required to form a closed

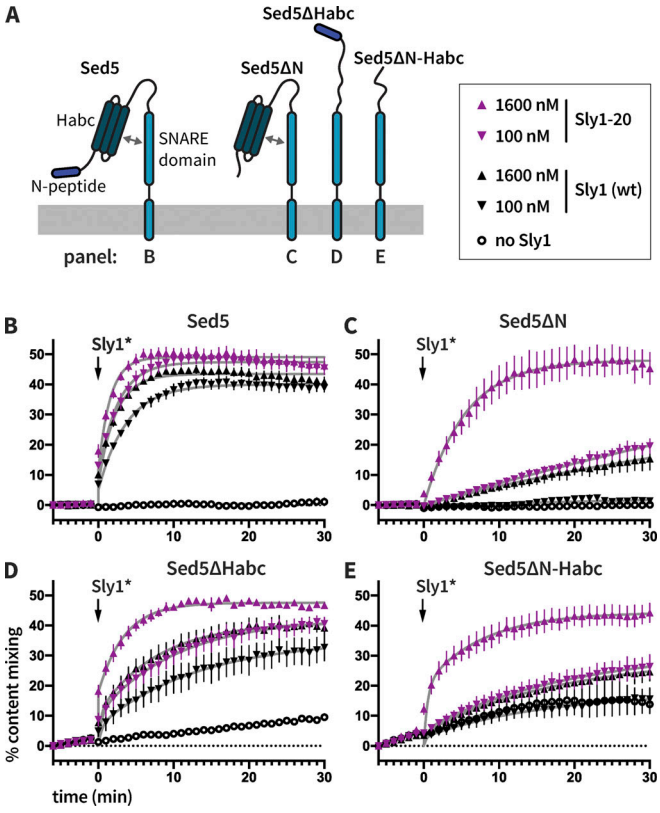

Figure 3. **Sly1 stimulates fusion driven by constitutively open Sed5. (A)** Diagram showing Sed5 constructs used in this figure. Sed5ΔN lacks residues 1–21. Sed5 ΔHabc lacks residues 51–180. Sed5ΔN-Habc lacks residues 1–180. **(B–E)** Sly1 and Sly1-20 stimulation of fusion by RPLs bearing the Sed5 mutants indicated. At t = −6 min, reactions were initiated with the indicated RPLs in the presence of 3% PEG, 100 nM Sec17, 100 nM Sec18, and 1 mM Mg·ATP. At t = 0, Sly1 or Sly1-20 was added to the reactions at 0, 100, or 1,600 nM, as indicated in the legend in the upper right corner. Points show mean ± SEM of at least three independent experiments. Gray lines show least-squares fits of a second-order kinetic function.

conformation but retains the N-terminal 21 amino acids that bind Sly1 with high affinity. Sed5ΔN-Habc lacks both the N-peptide and the Habc domain.

Both *sed5ΔHabc* and *sed5ΔN-Habc* confer recessive lethal phenotypes. The lethality of these alleles was not suppressed by the expression of *SLY1* or *SLY1-20* from single- or multiple-copy plasmids (Fig. S2 A). The protein products of these *sed5* alleles are synthesized (Fig. S2 B). However, the mutant Sed5 proteins mislocalize and are degraded in the lumen of the lysosomal vacuole (Fig. S2 C). The Habc domain therefore contains information essential for correct Sed5 localization and in vivo function. A more detailed analysis of Sed5 localization determinants is presented elsewhere (Gao and Banfield, 2020).

To assess the role of Sed5 autoinhibition in membrane fusion, we returned to the in vitro RPL assay system. As above, RPLs bearing wild-type Sed5 or Sed5ΔN exhibited little or no fusion when Sly1 was absent (Fig. 3, B and C; black open circles). In contrast, RPLs bearing either Sed5ΔHabc or Sed5ΔN-Habc exhibited spontaneous but slow Sly1-independent fusion (Fig. 3, D and E; black open circles). These results strongly corroborate solution biochemistry studies which indicate that autoinhibition of Sed5 by its Habc domain blocks SNARE complex assembly and therefore fusion (Demircioglu et al., 2014). In the presence of Sly1 or Sly1-20, however, fusion was stimulated by Sly1 whether the Habc domain was present (Fig. 3, B and C) or absent (Fig. 3, D and E). Thus, while one function of Sly1 is to open the Sed5 closed conformation, Sly1 must have additional fusion-promoting activities.

Wild-type Sly1 requires an extrinsic tethering activity to stimulate fusion

In our experiments and previous work, wild-type Sly1 stimulates SNARE-mediated fusion only in the presence of native tethers or, alternatively, polyethylene glycol (PEG). At high concentrations (20–30%), PEG can directly trigger fusion. At far lower concentrations in our reactions (3–4%), PEG aggregates or tethers vesicles without fusion (Dennison et al., 2006; Lentz, 2007). Because PEG is a crowding agent, the question arises as to whether protein-mediated tethering might be sufficient to enable Sly1-mediated fusion or, alternatively, whether microscopic volume exclusion or crowding effects of PEG are more important. To distinguish between these possibilities, we used a synthetic protein tether, GST-P4MKA. P4M, a domain within the *Legionella* effector protein SidM/DrrA, binds to the headgroup of phosphatidylinositol-4-phosphate (PI4P), present in the RPLs used in our fusion reactions (Del Campo et al., 2014). When fused to glutathione S-transferase (GST), which homodimerizes, P4M is presented on opposite sides of the GST dimer, potentially spanning and tethering liposomes. A similar approach was used in the reconstitution of yeast vacuole fusion (Song and Wickner, 2019).

To test whether GST-P4M can function as a tether, we used bead-based and dynamic light scattering assays. Liposomes doped with PI4P and marked by a fluorescent lipid were prepared by extrusion through a ∼200 nm polycarbonate filter. Bead-based assays were performed by decorating glutathione–sepharose beads with GST-P4M and adding the liposomes, to see if liposomes bound to the decorated beads (Fig. 4 A). When viewed by confocal microscopy (Fig. 4 B), beads decorated with GST-P4M weakly bound liposomes. Surprisingly, a P4M mutant with de-tuned affinity, GST-P4MKA, tethered vesicles much more efficiently. GST-P4MKA was further examined in a dynamic light scattering (DLS) assay of tethering (Lo et al., 2011). Individual liposomes behave as ∼200 nm particles, while clusters of tethered liposomes behave as larger particles that diffuse more slowly and scatter more intensely (Fig. 4 C). As in the bead assays, GST-P4MKA tethered robustly at 1–5 µM, consistent with the ∼10 µM affinity of P4MKA (Del Campo et al., 2014). Cleavage of GST-P4MKA with 3C protease (Fig. 4 A) releases P4MKA monomer from the GST dimer. 3C cleavage of GST-P4M abolished tethering (Fig. 4 C). P4M therefore must be dimerized to mediate tethering.

GST-P4MKA facilitated efficient Sly1-dependent fusion in the absence of PEG (Fig. 4 D). As in the tethering assays, this occurred over a concentration range consistent with ∼10 µM affinity of P4MKA for PI(4)P. Dimerization of P4MKA was essential for its ability to stimulate fusion (Fig. 4 E), as monomerization by 3C protease cleavage abolished fusion. In an

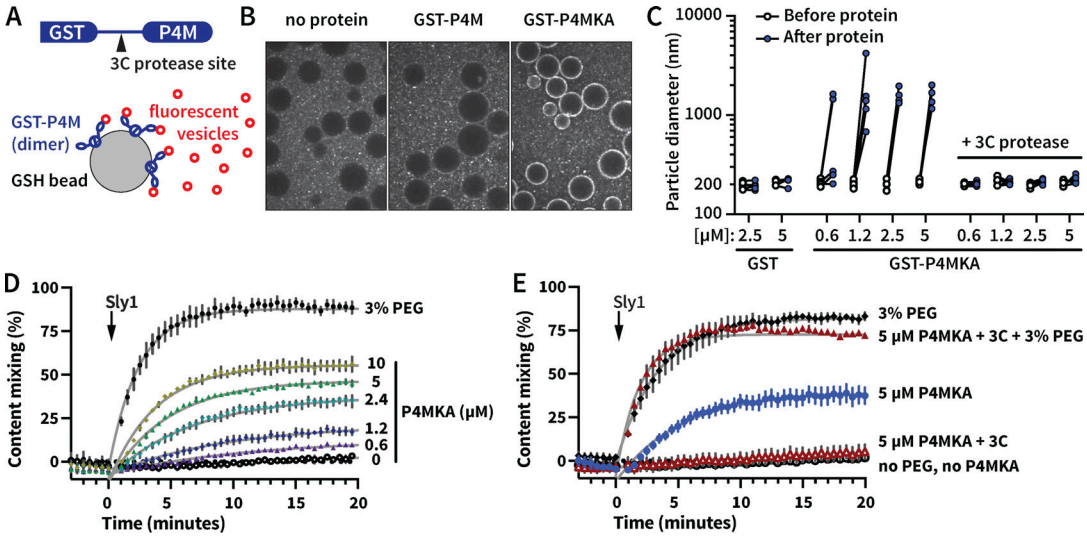

Figure 4. **A synthetic protein tether promotes Sly1-mediated fusion. (A)** Cartoon representation of GST-P4M constructs and bead-based tethering assay (not drawn to scale). The GST affinity tag is dimeric and binds to affinity beads displaying reduced glutathione (GSH). **(B)** GST-P4M and GST-P4MKA tether vesicles to beads. GSH beads are large dark spheres. Vesicles tethered to beads are visible as fluorescent halos around the beads. **(C)** Dimeric GST-P4MKA tethers vesicles in solution. Homotypic tethering was monitored by dynamic light scattering. ~200 nm vesicles were measured before and after the addition of the indicated proteins. Increasing particle diameter indicates the presence of clusters of vesicles. **(D)** GST-P4MKA promotes Sly1-dependent membrane fusion in the absence of PEG. **(E)** P4MKA must be dimeric to mediate tethering. Points show mean ± SEM of at least three independent experiments. Gray lines show least-squares fit of a second-order kinetic function.

important control, fusion was restored by 3% PEG, showing that 3C protease and monomeric P4MKA do not themselves block fusion. Together, these experiments show that vesicle tethering is necessary for Sly1-dependent fusion. Additional crowding or excluded volume effects therefore are not essential. However, fusion is somewhat more efficient with PEG than with GST-P4MKA.

Sly1 can stimulate fusion independently of both Sed5 opening and Sly1-mediated close-range tethering

An autoinhibitory loop conserved among Sly1 family members harbors a close-range vesicle tethering activity, which is indispensable for the hyperactivity of the Sly1-20 mutant (Duan et al., 2024). We, therefore, asked if Sly1 can stimulate fusion independently of both its close-range tethering function and its ability to open the Sed5 closed conformation. Reactions were initiated with RPLs bearing Sed5ΔHabc (which cannot adopt a closed conformation) and with wild-type Sly1 or Sly1 mutants defective in close-range tethering (Fig. 5 A). The Sly1Δloop mutant lacks the entire Sly1-specific regulatory loop, including the amphipathic helix α21, which is required for close-range membrane tethering. When Sly1Δloop was added to reactions containing Sed5-ΔHabc RPLs, an increase in fusion was still observed, indicating that Sly1 must have fusion-stimulating activities beyond Sed5 opening and close-range tethering.

This conclusion was buttressed by two additional Sly1 mutants. In the Sly1pα21 protein, five apolar residues within helix α21 are mutated, preventing the loop from binding to membranes. Sly1-pα21 has at least two functional defects: it is constitutively autoinhibited, and it is defective for close-range tethering (Duan et al., 2024). As expected, Sly1-pα21 stimulated only barely detectable fusion above the background (Fig. 5 A). In the compound mutant Sly1-20-pα21, autoinhibition is released (the loop is open), but close-range tethering is still compromised. When added to reactions with Sed5ΔHabc RPLs, Sly1-20-pα21 stimulated fusion similarly to the Sly1Δloop (Fig. 5 A). When the same set of Sly1 variants was tested with Sed5ΔHabc RPLs under tethering-deficient conditions (Fig. 5 B), only Sly1-20 (constitutively open and presenting helix α21) was able to stimulate substantial fusion. Thus, fusion of Sed5ΔHabc RPLs requires a tethering activity that can be provided either by the tethering-hyperactive Sly1-20 or by extrinsic tethering agents. We conclude that both Sly1 opening of closed Sed5 and Sly1 close-range tethering activity contribute to the ability of Sly1 to promote fusion, and that Sly1 also promotes fusion independently of these two activities. In Vps33 and Munc18-1, domain 3a appears to serve as a template for trans-SNARE complex assembly (Baker et al., 2015; Jiao et al., 2018; Parisotto et al., 2014; Stepien et al., 2022). The near-inability of the constitutively autoinhibited mutant Sly1-pα21 to stimulate fusion (Fig. 5 A) implies that additional Sly1 activities involve Sly1 domain 3a, which is occluded when Sly1 is autoinhibited, as shown by crystal structures and modeling (Baker et al., 2015; Bracher and Weissenhorn, 2002; Duan et al., 2024).

Sly1 close-range tethering promotes the assembly of trans-SNARE complexes

The assembly of cis-SNARE complexes occurs spontaneously and competes with the assembly of fusion-active trans-SNARE complexes. We hypothesized that close-range tethering by Sly1 specifically favors trans-SNARE complex assembly. To test this idea, we compared Sly1 and Sly1 mutants with altered tethering activity in fusion reactions challenged by a soluble R-SNARE domain, $Sec22_{SN}$-GFP. This soluble R-SNARE

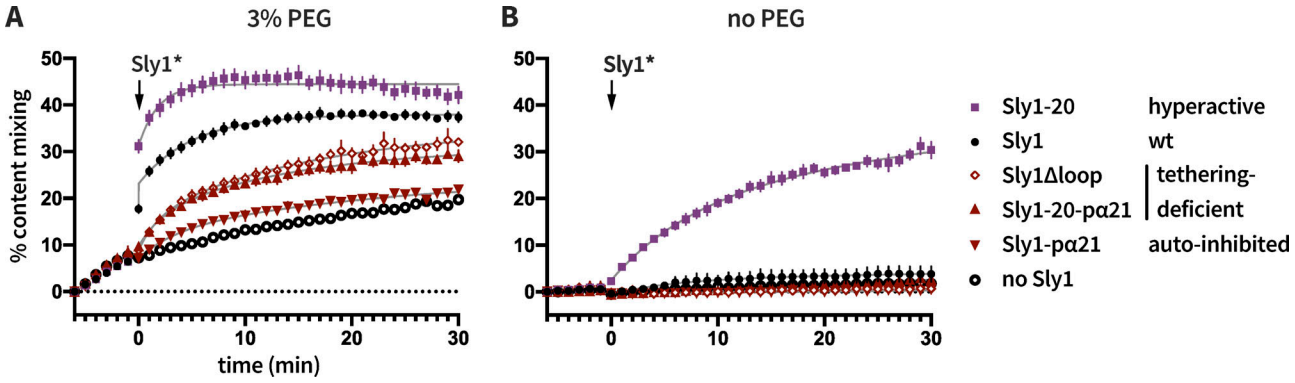

Figure 5. **Sly1 can stimulate fusion independently of both Sed5 opening and close-range tethering.** At t = −6 min, reactions were initiated with R-SNARE RPLs, Q-SNARE RPLS bearing Sed5ΔHabc, 100 nM Sec17, 100 nM Sec18, and 1 mM Mg·ATP. **(A and B)** The reactions also contained (A) 3% PEG or (B) 0% PEG. At t = 0, the indicated Sly1* variants were added to 1,600 nM final, as indicated in the legend. Points show mean ± SEM of at least three independent experiments. Gray lines show least-squares fit of a second-order kinetic function.

domain is predicted to form fusion-dead cis-SNARE complexes with the Qa, Qb, and Qc SNAREs on the RPLs.

Reactions were initiated with RPLs bearing the three Q-SNARES along with $Sec22_{SN}$-GFP (0, 2 or 20 μM), and either wild-type or mutant forms of Sly1. Sec17, Sec18, and ATP were also present. These mixtures were incubated for 15 min to dissociate any cis-Q-SNARE complexes present. Then R-SNARE RPLs were added. This mixture was incubated for an additional 6 min to allow complete mixing of the two RPL populations and to determine whether any PEG-independent fusion occurred. PEG was then added to initiate fusion (t = 0). Here, PEG was used at 4% rather than 3% (as in previous experiments) to compensate for tethering defects of the Sly1-20-α21p and Sly1Δloop mutants. In the absence of $Sec22_{SN}$-GFP and with 4% PEG (Fig. 6 A), the tethering-deficient Sly1 mutants mediated fusion almost as efficiently as wild-type Sly1 or hyperactive Sly1-20. Fusion at 2 μM $Sec22_{SN}$-GFP was partially inhibited with tethering-deficient Sly1* mutants (Fig. 6 B), but there was no detectable inhibition of fusion with wild-type Sly1 or tethering-hyperactive Sly1-20. This difference was even more pronounced in the presence of 20 μM $Sec22_{SN}$-GFP (Fig. 6 C): fusion was partially inhibited in Sly1 and Sly1-20 reactions but almost eliminated in reactions with tethering-deficient Sly1 mutants.

Sec17/18 enhanced the resistance of Sly1-mediated fusion to inhibition by $Sec22_{SN}$-GFP. In control reactions lacking Sec17 and Sec18, fusion was more strongly inhibited by $Sec22_{SN}$-GFP with all Sly1 variants, including the wild type (Fig. S3, A–C). This was expected because Sec17 and Sec18 are needed to disassemble fusion-dead cis-SNARE complexes containing $Sec22_{SN}$-GFP. Additionally, experiments with PEG at 3% rather than 4% yielded generally similar results (Fig. S3, D–I). Taken together, these experiments support the hypothesis that close-range tethering by Sly1 biases assembly toward fusogenic trans-SNARE complexes rather than non-fusogenic cis-SNARE complexes, even when nonspecific vesicle membrane aggregation is strongly driven by 4% PEG.

We wondered if similar results might be obtained using wild-type membrane-anchored Sec22 rather than soluble $Sec22_{SN}$-GFP. We therefore assayed the fusion of 4-SNARE QabcR RPLs with 3-SNARE Qabc RPLs in the presence of wild type and mutant Sly1 variants (Fig. 7). QabcR RPLs can form quaternary SNARE complexes in cis, as they require Sec17/18 for efficient fusion, to liberate SNAREs that can then form fusogenic trans complexes. In this experimental geometry, the formation of trans-SNARE complexes and cis-SNARE complexes are competing processes. As above, we ran reactions in the presence of 4% PEG in an effort to compensate for the defects of tethering-deficient Sly1 mutants. Because Sly1 is recruited to the Qa-SNARE Sed5 through a high-affinity interaction with the Sed5 N-peptide, we used the Sed5ΔN mutant to bias Sly1 recruitment to either Qabc RPLs (Fig. 7 A) or QabcR RPLs (Fig. 7 B). Fusion is most efficient when Sly1 is placed on Sed5 in trans to the R-SNARE Sec22 (Fig. 7 A). Fusion is least efficient when Sed5-Sly1 is placed in cis to the R-SNARE (Fig. 7 B). Under each of these conditions, the tethering-deficient Sly1 mutants exhibit large defects (Compare Fig. 7, A–C versus Fig. 6 A). Tethering-deficient Sly1 variants were almost completely unable to drive fusion when the R-SNARE Sec22 and Sed5-Sly1 were all restricted to the same membrane (Fig. 7 B). To rule out the possibility that 100 nM Sly1* is subsaturating under these conditions, identical experiments were performed at 1,600 nM Sly1* (Fig. S4). Almost indistinguishable results were obtained. Taken together, these experiments demonstrate that the Sly1 close-range tethering activity takes on special importance when Sly1 catalysis of trans-SNARE complex assembly is in competition with the assembly of inactive cis-SNARE complexes.

The Sed5 Habc domain promotes SM-dependent fusion

In experiments comparing various Sed5 mutants, we were surprised to find that although Sed5ΔHabc is more active than wild-type Sed5 in Sly1-independent fusion reactions, its ability to support Sly1-stimulated fusion was decreased compared with the wild type (compare Fig. 3, B and D). This suggested that the Sed5 Habc domain, in addition to being autoinhibitory, might have a positive, fusion-promoting activity. To test that hypothesis, we asked if the Habc domain, supplied in soluble form, could alter the ability of Sly1 and its cognate SNAREs to drive fusion.

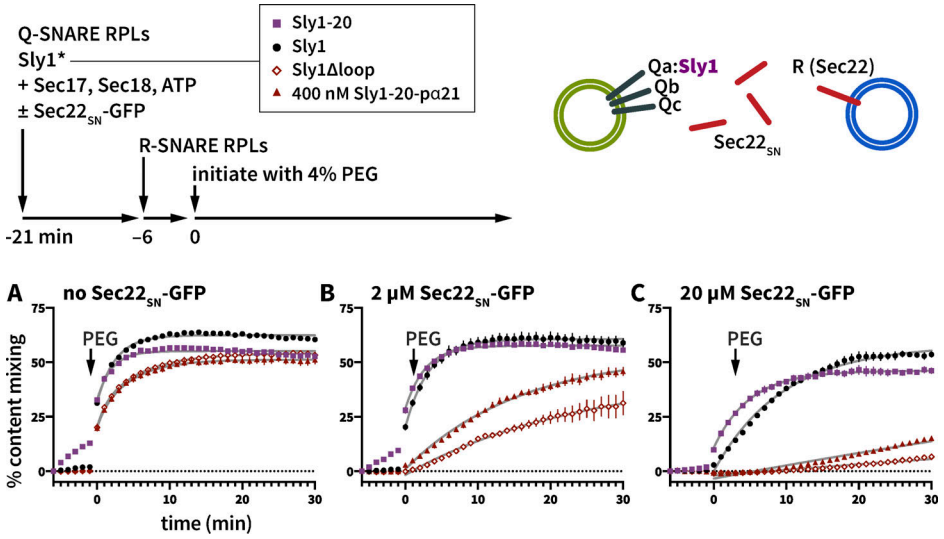

Figure 6. **Sly1 tethering helix α21 promotes selective formation of fusion-active trans-SNARE complexes. (A–C)** At t = −21 min, Q-SNARE RPLs bearing Sed5-WT were mixed with 100 nM SLY1 variants as indicated in the legend, Sec17/Sec18 (100 nM each), Mg·ATP (1 mM), and with either 0 μM (A), 2 μM (B) or 20 μM (C) soluble $Sec22_{SN}$-GFP. R-SNARE RPLs were added at t = −6 min. At t = 0, the reactions were initiated by adding 4% PEG. Points show mean ± SEM of at least three independent experiments. Gray lines show least-squares fit of a second-order kinetic function.

Reactions were initiated with Qabc-SNARE RPLs bearing four different Sed5 variants: wild-type, Sed5ΔN, Sed5ΔHabc, or Sed5 ΔN-Habc. Each reaction was performed in the absence or presence of either soluble Sed5 Habc or N-Habc domains (Fig. 8, A–D). Because Sly1 binds soluble N-Habc domain with subnanomolar affinity (Demircioglu et al., 2014), Sly1 and soluble Habc or N-Habc were premixed before being added together to the RPLs. The reactions were initiated without PEG and monitored for 6 min. To initiate fusion, PEG was added to 3% (t = 0). To our surprise, both the Habc and N-Habc domains of Sed5 stimulated fusion. Fusion was most efficiently stimulated when the N-peptide was present on the soluble Habc domain (Fig. 8 B). However, Habc stimulated fusion under every condition tested, even when the N-peptide was absent from both Sed5 and the soluble Habc domain (Fig. 8 D). The sole exception to this pattern was when N-Habc was added to reactions containing wild-type Sed5 on the RPLs (Fig. S5 E). Similar results were obtained in reactions with Sec17 and Sec18 (Fig. 8) or without (Fig. S5).

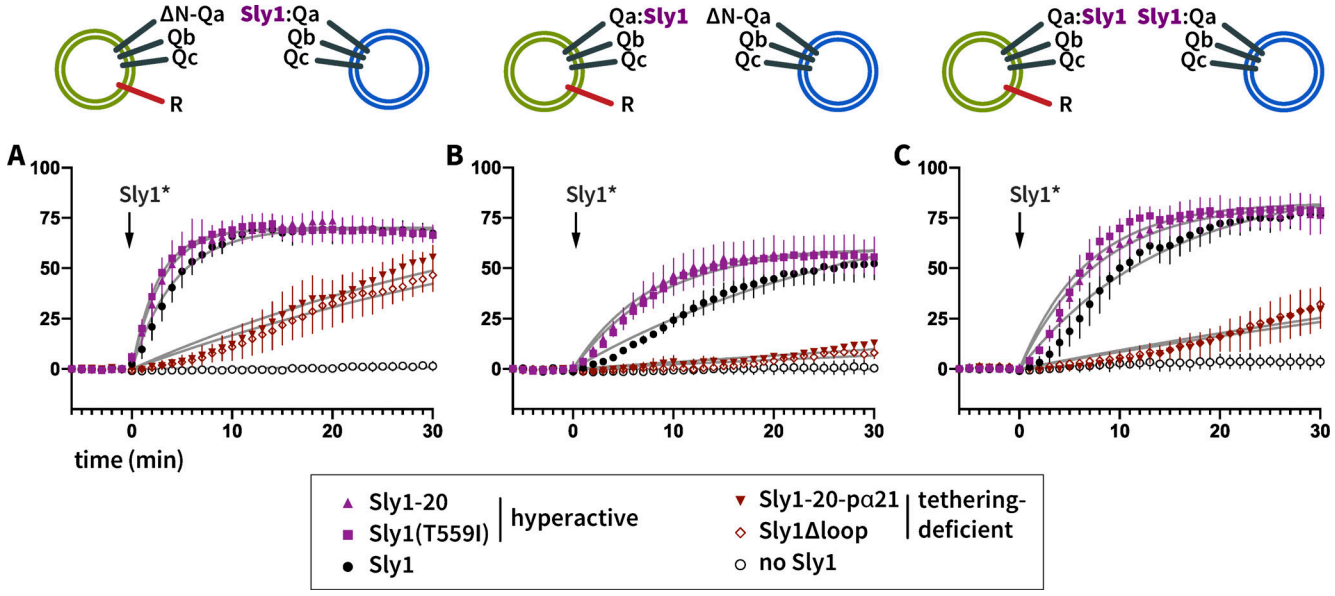

Figure 7. **Sly1 α21 promotes Sly1 discrimination between cis- and trans-SNARE complexes**. Reactions were initiated with RPLs bearing SNAREs in the indicated topologies. All reactions contained Sec17, Sec18 (100 nM each), and Mg^{2+}·ATP (1 mM). PEG was added to 4% final rather than 3% to assist the tethering-deficient Sly1 mutants. **(A–C)** Fusion was initiated (t = 0) by adding the indicated Sly1 mutants to 100 nM (A–C). Points show mean ± SEM of at least three independent experiments. Gray lines show least-squares fit of a second-order kinetic function.

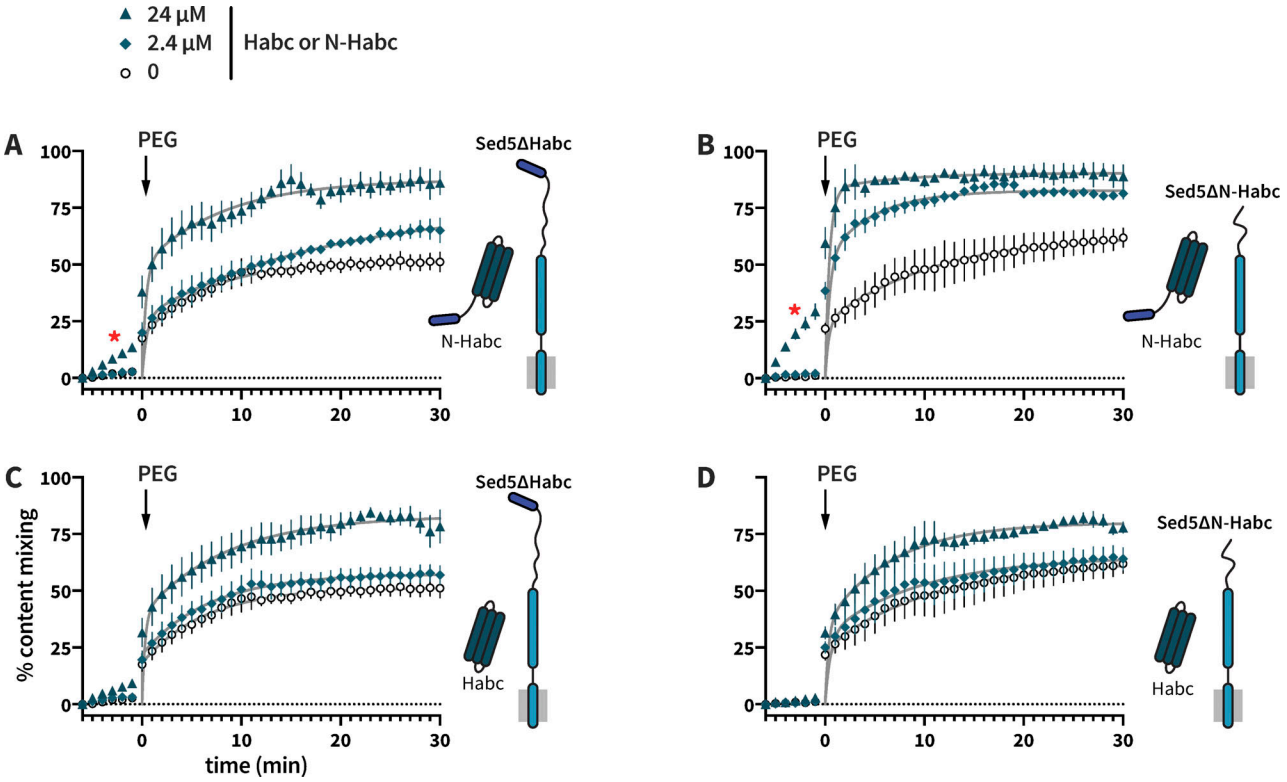

Figure 8. **Soluble Sed5 Habc domain can stimulate Sly1-dependent fusion in trans. (A–D)** At t = −6 min, R-SNARE RPLs and Q-SNARE RPLS bearing either Sed5ΔHabc (A and C) or Sed5ΔN-Habc (B and D) were mixed with Sec17, Sec18 (100 nM), and Mg^{2+}·ATP (1 mM), and 1.5 μM Sly1 that had been preincubated with the indicated concentrations of soluble Sed5N-Habc (A and B) or Sed5Habc (C and D). At t = 0, reactions were initiated by the addition of 3% PEG. Points show mean ± SEM of at least three independent experiments. Gray lines show least-squares fit of a second-order kinetic function. In A and B, red asterisks (*) indicate fusion that occurred prior to the addition of PEG. Similar experiments performed without Sec17 and Sec18, and also with wild-type Sed5, are shown in Fig. S5.

Remarkably, in the presence of Sec17 and Sec18, and at the highest concentration of N-Habc, fusion was initiated even before PEG was added to the reaction (Fig. 8, A and B; red asterisks). This indicates a bypass of the tethering requirement—a result previously obtained only with hyperactive Sly1 mutants such as Sly1-20 (Duan et al., 2024). We conclude that the Sed5 Habc domain augments the efficiency of Sly1-stimulated fusion and that the Habc domain need not be covalently coupled to Sed5. In other words, "split Sed5" can stimulate fusion with the Habc fragment presented separately from the SNARE motif.

To assess at what stage the Habc domain promotes fusion, we compared the lipid and content mixing trajectories for sets of reactions. If Habc promotes the onset of lipid mixing but does not regulate subsequent opening of a stable fusion pore, we expect lipid and content mixing to correlate since pore opening should not be influenced by the absence or presence of Habc. On the other hand, if Habc promotes opening or stability of the fusion pore, we expect reactions where Habc is absent to accumulate intermediates with lipid but not content mixing. First, we compared fusion reactions with RPLs bearing either wild-type Sed5 or Sed5ΔHabc, stimulated by either Sly1 or Sly1-20 (Fig. S6). Second, we compared fusion reactions with Sed5ΔN-Habc RPLs, with and without the addition of the soluble N-Habc fragment (Fig. S7). In each case, the lipid and content mixing signals were correlated. Thus, the Sed5 Habc domain mainly stimulates fusion at stages prior to or during lipid mixing. If Habc contributes to the formation of a stable fusion pore downstream of lipid mixing, that contribution is relatively minor.

Soluble Sed5 Habc domain promotes Sly1-stimulated fusion in vivo

Next, we tested whether soluble Sed5 Habc or N-Habc domains might suppress the lethal phenotype of cells expressing Sed5 variants lacking these features (Fig. 9). Single-copy bicistronic plamids were constructed bearing *sed5ΔN-Habc* or *sed5ΔHabc*, as well as either *Habc* or *N-Habc*. These test plasmids were introduced into *sly1Δ sed5Δ* strains harboring a counter-selectable *SLY1 SED5* balancer plasmid. In vitro, we had noted that Qabc RPLs bearing wild-type Sed5 fuse with similar efficiency when either Sly1 or hyperactive Sly1-20 are supplied, but that RPLs bearing Sed5ΔHabc are considerably more responsive to Sly1-20 (Fig. 3). Thus, we also tested the effects of single-copy or multiple-copy plasmids bearing either *SLY1* or *SLY1-20*. The results show that the Sed5 N-Habc domain can support viability when present solely as a soluble fragment (Fig. 9, A and B). However, the viability of these split Sed5 cells requires Sly1 hyperactivity. Only *SLY1-20* expressed from a high-copy vector supported robust growth with split Sed5. Single-copy *SLY1-20* supported very slow growth. Moreover, as in the in vitro assays, the rescue was most robust when the N-peptide was on the

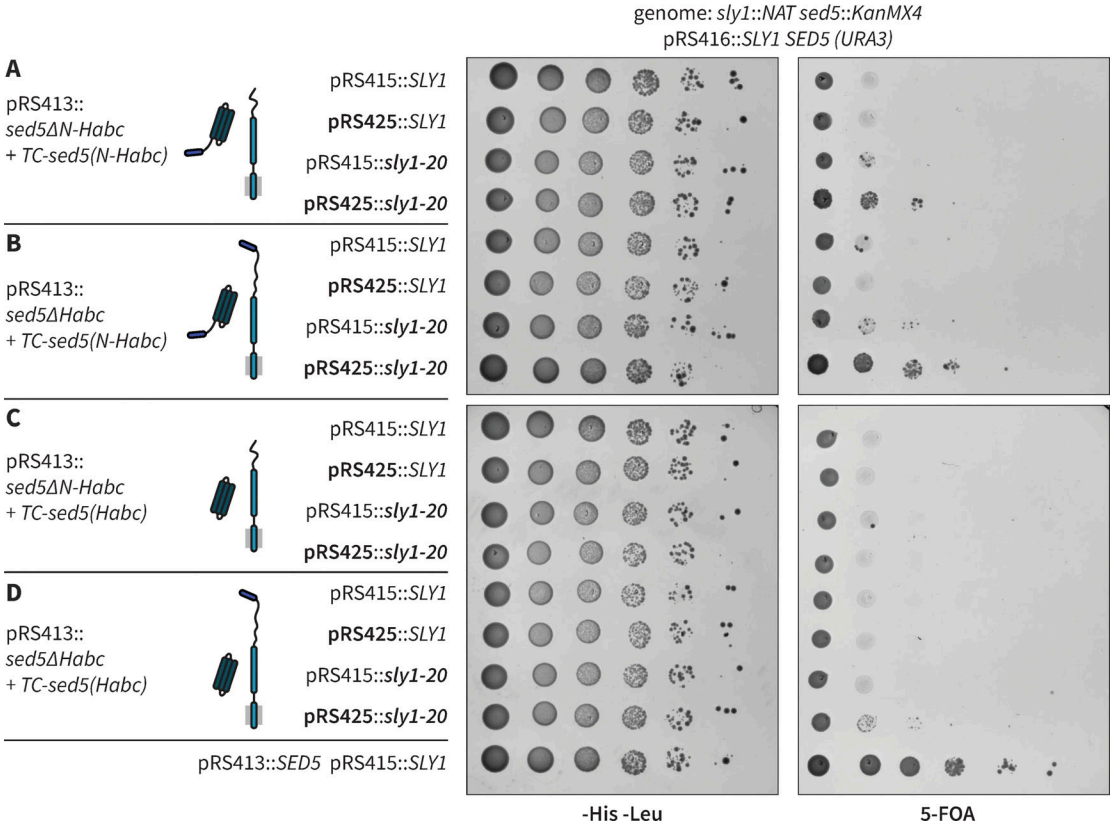

Figure 9. **Soluble Sed5 N-Habc fragment supports the viability of cells in the presence of *SLY1-20*.** Cells with the indicated genotypes **(A–D)** were constructed as described in the text. These strains were grown in –His –Leu liquid media to maintain the plasmids. Serial dilutions were then plated to either –His –Leu solid media or to solid media containing 5-FOA, to eject the *SLY1 SED5* balancer plasmid. Expression of the membrane-anchored Sed5 variants was driven using the native *SED5* promoter and terminator. Plasmids using the high-copy pRS425 backbone are indicated in bold type. All others are single-copy. Expression of the soluble Habc and N-Habc fragments of Sed5 was driven using the *TPI1* promoter and the *CYC1* terminator (*TC*). Immunoblot analyses of Sed5* expression in these cells are shown in Fig. S8.

soluble Habc fragment (Fig. 9, A and B). No rescue was observed in cells totally lacking the Sed5 N-peptide (Fig. 9 C), and rescue was only barely detectable when the N-peptide was present solely on the membrane-anchored mutant Sed5 (Fig. 9 D).

Immunoblot analyses of whole cell lysates from cells expressing wild-type Sed5 indicated that the truncated Sed5 variants and soluble fragments were expressed (Fig. S8 A). In cells lacking the *SLY1 SED5* balancer plasmid and expressing either Sed5ΔN-Habc or Sed5ΔHabc, the steady-state level of the soluble N-Habc fragment depended on the gene dosage of *SLY1-20*, suggesting that the stability of the soluble fragment is controlled by its interaction with Sly1-20 protein (Fig. S8 B). Taken together, the in vitro and in vivo results here and elsewhere (Gao and Banfield, 2020) indicate that, in addition to being autoinhibitory, the Sed5 Habc domain has positive functions: it both promotes Sly1-dependent membrane fusion and regulates Sed5 localization.

Discussion

Our experiments show that Sly1 has multiple experimentally separable activities, each of which promotes SNARE-mediated fusion. A working model with structural hypotheses generated using AlphaFold2 is presented in Fig. 10. First, Sed5-bound Sly1 has the intrinsic ability to tether incoming vesicles through the amphipathic helix α21 within the Sly1 regulatory loop (Duan et al., 2024). Second, Sly1 has the ability to open the closed, autoinhibited conformation of the Qa-SNARE Sed5 (Demircioglu et al., 2014). When these activities are nullified, Sly1 still promotes fusion (albeit less efficiently) through a third activity. We infer that this activity is nucleation of trans-SNARE complex assembly. This activity is strongly enhanced by the Sed5 Habc domain. These activities are interlinked.

Defects in the Sly1 close-range tethering function result in dramatically impaired fusion when cis-SNARE and trans-SNARE complex assembly are competing processes, indicating that the tethering function is closely coupled to selective catalysis of the trans-SNARE complex assembly. Although the precise mechanism through which this occurs is not rigorously established, structural data are suggestive. Assuming that the R-SNARE Sec22 binds to Sly1 in a configuration similar to the binding of R-SNARE Nyv1 to Vps33 (Baker et al., 2015), the open Sly1 loop should tether the incoming vesicle in an orientation optimal for the capture of the vesicular R-SNARE (Fig. 10 B). We therefore suggest that the close-range tethering mechanism serves not only to interrogate the biophysical properties of the

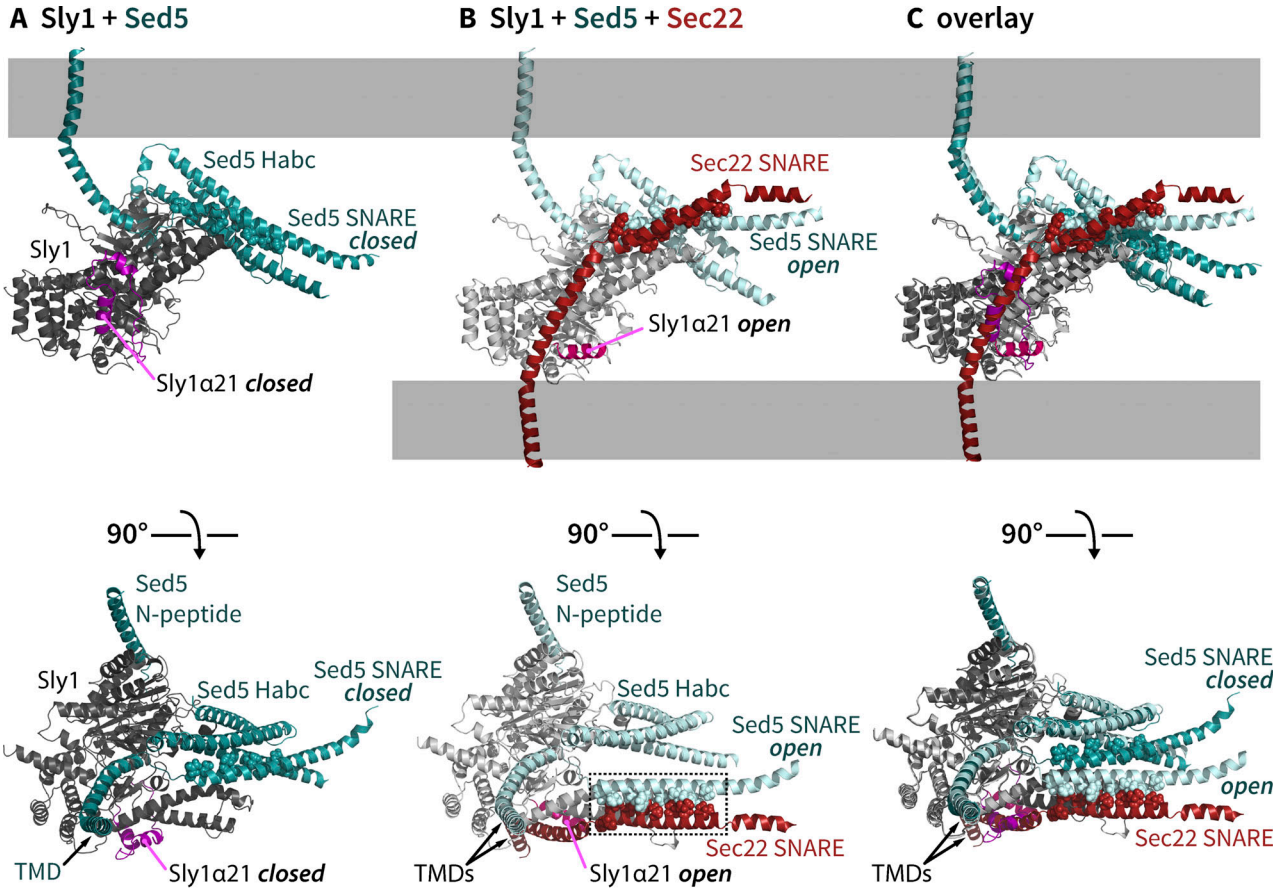

Figure 10. **AlphaFold2-based working model of Sly1-mediated *trans*-SNARE complex assembly. (A)** Sly1-Sed5 complex on Golgi target membrane. In this, rendering the Sly1 autoinhibitory loop is closed, and the Sed5 SNARE domain is also in a closed conformation associated with the Sed5 Habc domain. TMD, transmembrane domain. Disordered linkers are omitted for clarity. **(B)** Incipient trans-SNARE complex. In a working model, the following events occur. (i) Sly1 binds the Sed5 N-peptide. (ii) Sly1 binds the closed Sed5 Habc and SNARE bundle. (iii) Based on studies showing that Sly1 can open the Sed5 closed conformation (Demircioglu et al., 2014), we hypothesize that when bound to Sly1, Sed5 fluctuates between the fully closed conformation depicted in A and a partially open conformation like that seen in B, as well as in the Vps45-Tlg2 crystal structure (Eisemann et al., 2020). (iv) Sly1α21 binds the incoming vesicle's lipid bilayer. On the basis of crystallographic and biochemical data (Bracher and Weissenhorn, 2002; Duan et al., 2024), we hypothesize that the Sly1 autoinhibitory loop explores both open and closed conformations, with α21 probing for the presence of an incoming vesicle membrane. (v) α21 binding to the vesicle leaves the R-SNARE binding site on Sly1 open, allowing Sec22 binding; (vi) The N-terminal half of the Sec22 SNARE domain becomes partially structured on the Sly1 templating domain; (vii) SNARE zippering initiates as the Sec22-Sly1 complex engages the open conformation of Sed5 (dashed box in panel B). (viii) Quaternary trans-SNARE complex assembly, terminal zippering, and fusion ensue. **(C)** The hypothesized assembly states in A and B are overlaid. This comparison suggests that the hydrophobic packing layers of the Sed5 SNARE helix (shown as spheres on SNARE packing residues from helical turn −7 to the ionic "zero layer") would roll through 180° as Sed5 transits from its closed conformation to the open and partially zipped conformation. We further speculate that the Sed5 Habc domain, by prestructuring the Sed5 SNARE domain and placing it in the correct helical register, accelerates the formation of the Sed5-Sec22 template complex. AlphaFold2 modeling was done as described (Duan et al., 2024).

incoming vesicle membrane and trigger Sly1 activation but also to steer Sly1 into a spatial orientation that maximizes the likelihood of productive R-SNARE capture and trans-SNARE templating by domain 3a.

At the neuronal presynaptic membrane, the SM UNC-18/Munc18-1 seems to lock its Qa-SNARE Syntaxin-1A into a closed conformation. Another protein, UNC-13/Munc13-1 appears primarily responsible for opening syntaxin-1A (Richmond et al., 2001; Wang et al., 2017; Yang et al., 2015). However, it is unclear if UNC-13 is a synapse-specific elaboration or if proteins like UNC-13 are generally required for Qa-SNARE opening (Pei et al., 2009). Like Syntaxin-1A, the ER-Golgi Qa-SNARE Sed5 is autoinhibited. In contrast to Munc-18, Sly1 opens the closed Qa-SNARE, as does Vps45 with its cognate Qa-SNARE (Demircioglu et al., 2014; Eisemann et al., 2020). Nevertheless, Sly1 stimulates fusion even with Sed5ΔHabc mutants that cannot close. This had not previously been shown but was, perhaps, expected. Although all Qa (syntaxin-family) SNARE proteins have trihelical Habc domains, Habc domains are not always autoinhibitory. However, SM proteins are universally required. For example,

Vam3, the Qa-SNARE of the yeast lysosomal vacuole, is constitutively open. The Vam3 Habc domain lacks a groove that might fold back on its SNARE domain; yet its SM, Vps33, is still indispensable for fusion (Baker et al., 2015; Dulubova et al., 2001; Lobingier et al., 2014; Rieder and Emr, 1997; Seals et al., 2000). In addition to the above functions, Sly1 decreases the rate of SNARE complex disassembly by Sec17 and Sec18 (Lobingier et al., 2014). This is consistent with studies of Vps33 and Munc18-1, showing that these SMs protect assembled trans-SNARE complexes from premature disassembly by Sec17 and Sec18 (Duan et al., 2024; Lobingier et al., 2014; Prinslow et al., 2019; Schwartz et al., 2017; Song et al., 2017; Stepien et al., 2019; Xu et al., 2010).

We were somewhat surprised to find that Sly1-dependent fusion driven by Sed5ΔHabc is slower than the fusion driven by wild-type Sed5. Similarly, deletion of the Vam3 Habc domain causes a kinetic defect in homotypic vacuole fusion (Laage and Ungermann, 2001; Lürick et al., 2015; Pieren et al., 2010), though there is a contradictory report (Wang et al., 2001). When we added soluble Habc domain to reactions containing Sed5ΔHabc RPLs, fusion activity was restored to wild-type or nearly wild-type levels (Fig. 8). The Habc domain of Sed5 therefore must have a positive function.

What could that function be? Pieren et al. (2010) suggested that the Vam3 Habc domain, through interaction with Vps33, facilitates a transition from lipid to content mixing. However, we have detected no signals consistent with the hypothesis that the Sed5 Habc domain promotes that late step. Experiments from the Zhang laboratory are more suggestive of an underlying mechanism. Using single-molecule force spectroscopy, they probed the formation and stability of template complexes consisting of neuronal SNAREs and the cognate SM Munc18-1 (Jiao et al., 2018; Yang et al., 2022). Formation of the SNARE–Munc18-1 template complex was almost an order of magnitude less efficient when Syntaxin 1A lacked its N-terminal regulatory domain (the N-peptide and Habc domain). In a striking parallel to our fusion experiments, the addition of soluble N-Habc domain rescued template complex formation and increased the stability of the template complex (Jiao et al., 2018). Recent Vps45 and Munc18-1 structures (Eisemann et al., 2020; Stepien et al., 2022) and our AlphaFold2 modeling further suggest the possibility that Sly1-bound Sed5 exists in both closed and open states (Fig. 10, A and B). Habc interactions would place the "zero layer" of the Sed5 SNARE domain in a precise phase and with a 180° roll of the SNARE domain, axial registration with Sec22 on the Sly1 template, contributing to the assembly of stable and productive template complexes upon Sec22 binding (Fig. 10 C).

We reiterate our previous suggestions (Lobingier et al., 2014; Schwartz et al., 2017) that SM proteins are, sensu stricto, enzymes. Like all enzymes, SMs bind substrates (vesicular and target SNARE domains), placing them in a stereoselective orientation that reduces the kinetic barrier to the formation of the product (the trans-SNARE complex). The SMs then dissociate from the product to engage in additional cycles of catalysis (Jiao et al., 2018; Schwartz et al., 2017). Also, as expected for true enzymes, SMs prevent off-pathway reactions (e.g., assembly of non-cognate SNARE complexes or cis- rather than trans-complexes). SMs achieve this increase in specificity through two mechanisms. Kinetic partitioning favors formation of correct complexes within the forward assembly pathway (Hardy and Randall, 1991; Lambright et al., 1994; Peng and Gallwitz, 2004; Lai et al., 2017). Kinetic proofreading by Sec17 and Sec18 selectively removes incorrect SNARE assemblies, while SMs selectively protect cognate trans-complexes from premature disassembly (Choi et al., 2018; Lobingier et al., 2014; Prinslow et al., 2019; Schwartz et al., 2017; Song et al., 2017; Xu et al., 2010). The enzymatic activities of SMs, Sec17, and Sec18 thus operate as a system to ensure efficient and accurate assembly and recycling of fusion complexes through cycles of docking and fusion.

Materials and methods

Yeast strains, genetic tests, and microscopy

Yeast and *E. coli* strains are listed in Table S1. Viability assays were performed as described (Gao and Banfield, 2020).

Proteins

Full-length SNAREs were expressed and purified as described (Duan et al., 2024). Constructs used to express mutant forms of Sed5 are listed in Table S1. Sed5 mutants bearing transmembrane domains were expressed and purified as for full-length wild-type Sed5. Soluble domains of Sed5 were expressed and purified as described (Duan et al., 2024). Sly1 and its mutants were expressed and purified as described (Duan et al., 2024). GST-H_6-(3C)-P4M(K568A) was expressed from the pET-49 vector in Rosetta2(DE3) cells. Starter cultures were grown overnight at 37°C in MDAG-135 media containing 100 mg/ml carbenicillin and 50 mg/ml chloramphenicol. 250 ml of ZYM-5052 autoinduction media with 100 mg/ml carbenicillin and 34 mg/ml chloramphenicol was inoculated with 1:500 dilution of starter culture and grown in an orbital shaker at 37°C and 285 rpm for 2 h. The culture was then transferred to a 30°C shaker and culture growth continued for another 13 h. Cells were pelleted at 4°C, resuspended in 25 ml of cold IMAC buffer supplemented with 30 mM imidazole, 0.25 mg/ml chicken egg lysozyme, 1× SigmaFAST Protease inhibitor cocktail, and 125 U Benzonase nuclease per gram of cell paste. Resuspended cells were lysed using an Emulsiflex-C5 high-pressure homogenizer (Avestin) and the lysate was clarified by centrifugation. Clarified lysate was incubated with Ni^{2+}-Sepharose HP (GE Healthcare) for ~30 min at 4°C. The resin was collected by flowing the clarified lysate through a disposable column and washed with 10 column volumes of IMAC buffer containing 65 mM imidazole. Protein was eluted with IMAC buffer containing 500 mM imidazole in 0.5 ml fractions. The most concentrated fractions were combined, and the buffer was exchanged into FB160M1 using a PD-10 column (GE Healthcare). Aliquots were snap-frozen in liquid nitrogen in thin wall PCR tubes and stored at −70°C.

RPLs and fusion assays

RPL lipid compositions, detailed methods for RPL preparation, and the setup and interpretation of the in vitro fusion assay are

described in the companion study (Duan et al., 2024). In this study, additional SNARE topologies were tested, as described in the Results. The molar protein:phospholipid ratio for 4-SNARE liposomes was 1:1,200, and 1:600 for Qabc and R SNARE RPLs, respectively. For certain experiments, as specified, reactions were set up with a non-standard order of reagent addition, and/or fusion was initiated by adding PEG rather than by adding Sly1 or its mutants. Note that positive and negative control traces are in some cases repeated between figure panels. These are shared controls from larger experiments with multiple treatments, executed in parallel.

Online supplemental material

Fig. S1 shows growth assays used to examine genetic interactions among the sed5-ΔN, SLY1, and SLY1-20 alleles. Fig. S2 shows that the Sed5 Habc domain is essential for viability and also required for correct Sed5 localization within the cell. Fig. S3 shows experimental variations and additional controls for the experiments shown in Fig. 6. Fig. S4 shows experimental variations and additional controls for the experiments shown in Fig. 7. Fig. S5 shows experiments like the ones in Fig. 8, except that Sec17 and Sec18 were omitted. This figure also shows results with RPLs bearing wild type Sed5. Fig. S6, related to Fig. 4, shows that deletion of the Sed5 Habc domain decreases overall fusion but does not cause accumulation of reaction intermediates that exhibit lipid but not content mixing. Fig. S7, related to Fig. 8, shows that the addition of Sed5 N-Habc domain has similar effects on content mixing, indicating that Habc acts to promote lipid mixing, upstream of aqueous fusion pore formation. Fig. S8 shows immunoblot results for steady-state in vivo protein levels of Sed5, Sed5 mutants, and Habc or N-Hbc domains under various conditions. Table S1 describes the plasmids and yeast strains used in this study.

Data availability

The data, as well as plasmids and yeast strains constructed for this study, are available from the corresponding author upon reasonable request. For plasmids and strains listed in Table S1 as "Banfield collection," please contact Dr. D.K. Banfield. We may ask that requestors pay shipment costs for materials.

Acknowledgments

We are grateful to Drs. R. Baker, I. Topalidou, and M. Zick for helpful advice and critical comments on the manuscript; and D. Beacham (Molecular Probes/Thermo Fisher Scientific, Eugene, OR, USA) for gifts of fluorescent reagents.

This work was funded by the National Institutes of Health/National Institute of General Medical Sciences R01 GM077349 and GM130644, by the University of Washington (A.J. Merz), and the Hong Kong Research Council GRF 16101718 and AoE/M-05/12-2 (D.K. Banfield).

Author contributions: Conceptualization: A.J. Merz, M. Duan, and D.K. Banfield; Data curation: A.J. Merz and D.K. Banfield; Formal Analysis: A.J. Merz, M. Duan, G. Gao, and D.K. Banfield; Funding acquisition: A.J. Merz and D.K. Banfield; Investigation: M. Duan, G. Gao, A. Lin, E.J. Mackey, D.K. Banfield, and A.J. Merz; Methodology: A.J. Merz, M. Duan, G. Gao, A. Lin, and D.K. Banfield; Project administration: A.J. Merz and D.K. Banfield; Supervision: A.J. Merz and D.K. Banfield; Visualization: A.J. Merz; Writing—original draft: A.J. Merz; Writing—review and editing: All authors.

Disclosures: The authors declare no competing interests exist.

Submitted: 17 January 2020
Revised: 20 December 2023
Accepted: 22 February 2024

References

Angers, C.G., and A.J. Merz. 2011. New links between vesicle coats and Rab-mediated vesicle targeting. *Semin. Cell Dev. Biol.* 22:18–26. https://doi.org/10.1016/j.semcdb.2010.07.003

Baker, R.W., P.D. Jeffrey, M. Zick, B.P. Phillips, W.T. Wickner, and F.M. Hughson. 2015. A direct role for the Sec1/Munc18-family protein Vps33 as a template for SNARE assembly. *Science.* 349:1111–1114. https://doi.org/10.1126/science.aac7906

Bombardier, J.P., and M. Munson. 2015. Three steps forward, two steps back: Mechanistic insights into the assembly and disassembly of the SNARE complex. *Curr. Opin. Chem. Biol.* 29:66–71. https://doi.org/10.1016/j.cbpa.2015.10.003

Bracher, A., and W. Weissenhorn. 2002. Structural basis for the Golgi membrane recruitment of Sly1p by Sed5p. *EMBO J.* 21:6114–6124. https://doi.org/10.1093/emboj/cdf608

Brenner, S. 1974. The genetics of Caenorhabditis elegans. *Genetics.* 77:71–94. https://doi.org/10.1093/genetics/77.1.71

Carpp, L.N., L.F. Ciufo, S.G. Shanks, A. Boyd, and N.J. Bryant. 2006. The Sec1p/Munc18 protein Vps45p binds its cognate SNARE proteins via two distinct modes. *J. Cell Biol.* 173:927–936. https://doi.org/10.1083/jcb.200512024

Carr, C.M., and J. Rizo. 2010. At the junction of SNARE and SM protein function. *Curr. Opin. Cell Biol.* 22:488–495. https://doi.org/10.1016/j.ceb.2010.04.006

Choi, U.B., M. Zhao, K.I. White, R.A. Pfuetzner, L. Esquivies, Q. Zhou, and A.T. Brunger. 2018. NSF-mediated disassembly of on- and off-pathway SNARE complexes and inhibition by complexin. *Elife.* 7:e36497. https://doi.org/10.7554/eLife.36497

Dascher, C., R. Ossig, D. Gallwitz, and H.D. Schmitt. 1991. Identification and structure of four yeast genes (SLY) that are able to suppress the functional loss of YPT1, a member of the RAS superfamily. *Mol. Cell. Biol.* 11:872–885. https://doi.org/10.1128/mcb.11.2.872-885.1991

Del Campo, C.M., A.K. Mishra, Y.-H. Wang, C.R. Roy, P.A. Janmey, and D.G. Lambright. 2014. Structural basis for PI(4)P-specific membrane recruitment of the Legionella pneumophila effector DrrA/SidM. *Structure.* 22:397–408. https://doi.org/10.1016/j.str.2013.12.018

Demircioglu, F.E., P. Burkhardt, and D. Fasshauer. 2014. The SM protein Sly1 accelerates assembly of the ER-Golgi SNARE complex. *Proc. Natl. Acad. Sci. USA.* 111:13828–13833. https://doi.org/10.1073/pnas.1408254111

Dennison, S.M., M.E. Bowen, A.T. Brunger, and B.R. Lentz. 2006. Neuronal SNAREs do not trigger fusion between synthetic membranes but do promote PEG-mediated membrane fusion. *Biophys. J.* 90:1661–1675. https://doi.org/10.1529/biophysj.105.069617

Duan, M., R.L. Plemel, T. Takenaka, A. Lin, B.M. Delgado, U. Natterman, D.P. Nickerson, J. Mima, E.A. Miller, and A.J. Merz. 2024. SNARE chaperone Sly1 directly mediates close-range vesicle tethering. *J. Cell Biol.* https://doi.org/10.1083/jcb.202001032

Dulubova, I., S. Sugita, S. Hill, M. Hosaka, I. Fernandez, T.C. Südhof, and J. Rizo. 1999. A conformational switch in syntaxin during exocytosis: Role of munc18. *EMBO J.* 18:4372–4382. https://doi.org/10.1093/emboj/18.16.4372

Dulubova, I., T. Yamaguchi, D. Arac, H. Li, I. Huryeva, S.W. Min, J. Rizo, and T.C. Sudhof. 2003. Convergence and divergence in the mechanism of SNARE binding by Sec1/Munc18-like proteins. *Proc. Natl. Acad. Sci. USA.* 100:32–37. https://doi.org/10.1073/pnas.232701299

Dulubova, I., T. Yamaguchi, Y. Gao, S.W. Min, I. Huryeva, T.C. Südhof, and J. Rizo. 2002. How tlg2p/syntaxin 16 "snares" Vps45. *EMBO J.* 21:3620–3631. https://doi.org/10.1093/emboj/cdf381

Dulubova, I., T. Yamaguchi, Y. Wang, T.C. Südhof, and J. Rizo. 2001. Vam3p structure reveals conserved and divergent properties of syntaxins. *Nat. Struct. Biol.* 8:258–264. https://doi.org/10.1038/85012

Eisemann, T.J., F. Allen, K. Lau, G.R. Shimamura, P.D. Jeffrey, and F.M. Hughson. 2020. The Sec1/Munc18 protein Vps45 holds the Qa-SNARE Tlg2 in an open conformation. *Elife*. 9:e60724. https://doi.org/10.7554/elife.60724

Fasshauer, D., R.B. Sutton, A.T. Brunger, and R. Jahn. 1998. Conserved structural features of the synaptic fusion complex: SNARE proteins reclassified as Q- and R-SNAREs. *Proc. Natl. Acad. Sci. USA*. 95: 15781–15786. https://doi.org/10.1073/pnas.95.26.15781

Fernandez, I., J. Ubach, I. Dulubova, X. Zhang, T.C. Südhof, and J. Rizo. 1998. Three-dimensional structure of an evolutionarily conserved N-terminal domain of syntaxin 1A. *Cell*. 94:841–849. https://doi.org/10.1016/S0092-8674(00)81742-0

Furgason, M.L., C. MacDonald, S.G. Shanks, S.P. Ryder, N.J. Bryant, and M. Munson. 2009. The N-terminal peptide of the syntaxin Tlg2p modulates binding of its closed conformation to Vps45p. *Proc. Natl. Acad. Sci. USA*. 106:14303–14308. https://doi.org/10.1073/pnas.0902976106

Furukawa, N., and J. Mima. 2014. Multiple and distinct strategies of yeast SNAREs to confer the specificity of membrane fusion. *Sci. Rep.* 4:4277. https://doi.org/10.1038/srep04277

Gao, G., and D.K. Banfield. 2020. Multiple features within the syntaxin Sed5p mediate its Golgi localization. *Traffic*. 21:274–296. https://doi.org/10.1111/tra.12720

Grabowski, R., and D. Gallwitz. 1997. High-affinity binding of the yeast cis-Golgi t-SNARE, Sed5p, to wild-type and mutant Sly1p, a modulator of transport vesicle docking. *FEBS Lett.* 411:169–172. https://doi.org/10.1016/S0014-5793(97)00720-5

Hanson, P.I., R. Roth, H. Morisaki, R. Jahn, and J.E. Heuser. 1997. Structure and conformational changes in NSF and its membrane receptor complexes visualized by quick-freeze/deep-etch electron microscopy. *Cell*. 90:523–535. https://doi.org/10.1016/S0092-8674(00)80512-7

Hardy, S.J., and L.L. Randall. 1991. A kinetic partitioning model of selective binding of nonnative proteins by the bacterial chaperone SecB. *Science*. 251:439–443. https://doi.org/10.1126/science.1989077

Hata, Y., C.A. Slaughter, and T.C.S. Südhof. 1993. Synaptic vesicle fusion complex contains unc-18 homologue bound to syntaxin. *Nature*. 366: 347–351. https://doi.org/10.1038/366347a0

Jahn, R., and D. Fasshauer. 2012. Molecular machines governing exocytosis of synaptic vesicles. *Nature*. 490:201–207. https://doi.org/10.1038/nature11320

Jiao, J., M. He, S.A. Port, R.W. Baker, Y. Xu, H. Qu, Y. Xiong, Y. Wang, H. Jin, T.J. Eisemann, et al. 2018. Munc18-1 catalyzes neuronal SNARE assembly by templating SNARE association. *Elife*. 7:e41771. https://doi.org/10.7554/eLife.41771

Karim, A.S., K.A. Curran, and H.S. Alper. 2013. Characterization of plasmid burden and copy number in Saccharomyces cerevisiae for optimization of metabolic engineering applications. *FEMS Yeast Res.* 13:107–116. https://doi.org/10.1111/1567-1364.12016

Kosodo, Y., Y. Noda, and K. Yoda. 1998. Protein-protein interactions of the yeast Golgi t-SNARE Sed5 protein distinct from its neural plasma membrane cognate syntaxin 1. *Biochem. Biophys. Res. Commun.* 250: 212–216. https://doi.org/10.1006/bbrc.1998.9288

Laage, R., and C. Ungermann. 2001. The N-terminal domain of the t-SNARE Vam3p coordinates priming and docking in yeast vacuole fusion. *Mol. Biol. Cell*. 12:3375–3385. https://doi.org/10.1091/mbc.12.11.3375

Lai, Y., U.B. Choi, J. Leitz, H.J. Rhee, C. Lee, B. Altas, M. Zhao, R.A. Pfuetzner, A.L. Wang, N. Brose, et al. 2017. Molecular Mechanisms of Synaptic Vesicle Priming by Munc13 and Munc18. *Neuron*. 95:591–607.e10. https://doi.org/10.1016/j.neuron.2017.07.004

Lambright, D.G., S. Balasubramanian, S.M. Decatur, and S.G. Boxer. 1994. Anatomy and dynamics of a ligand-binding pathway in myoglobin: The roles of residues 45, 60, 64, and 68. *Biochemistry*. 33:5518–5525. https://doi.org/10.1021/bi00184a021

Lentz, B.R. 2007. PEG as a tool to gain insight into membrane fusion. *Eur. Biophys. J.* 36:315–326. https://doi.org/10.1007/s00249-006-0097-z

Lo, S.Y., C.L. Brett, R.L. Plemel, M. Vignali, S. Fields, T. Gonen, and A.J. Merz. 2011. Intrinsic tethering activity of endosomal Rab proteins. *Nat. Struct. Mol. Biol.* 19:40–47. https://doi.org/10.1038/nsmb.2162

Lobingier, B.T., and A.J. Merz. 2012. Sec1/Munc18 protein Vps33 binds to SNARE domains and the quaternary SNARE complex. *Mol. Biol. Cell*. 23: 4611–4622. https://doi.org/10.1091/mbc.e12-05-0343

Lobingier, B.T., D.P. Nickerson, S.Y. Lo, and A.J. Merz. 2014. SM proteins Sly1 and Vps33 co-assemble with Sec17 and SNARE complexes to oppose SNARE disassembly by Sec18. *Elife*. 3:e02272. https://doi.org/10.7554/eLife.02272

Lürick, A., A. Kuhlee, C. Bröcker, D. Kümmel, S. Raunser, and C. Ungermann. 2015. The Habc domain of the SNARE Vam3 interacts with the HOPS tethering complex to facilitate vacuole fusion. *J. Biol. Chem.* 290: 5405–5413. https://doi.org/10.1074/jbc.M114.631465

Ma, L., A.A. Rebane, G. Yang, Z. Xi, Y. Kang, Y. Gao, and Y. Zhang. 2015. Munc18-1-regulated stage-wise SNARE assembly underlying synaptic exocytosis. *Elife*. 4:e09580. https://doi.org/10.7554/eLife.09580

Misura, K.M., R.H. Scheller, and W.I. Weis. 2000. Three-dimensional structure of the neuronal-Sec1-syntaxin 1a complex. *Nature*. 404: 355–362. https://doi.org/10.1038/35006120

Mitchison, T.J. 2019. Colloid osmotic parameterization and measurement of subcellular crowding. *Mol. Biol. Cell*. 30:173–180. https://doi.org/10.1091/mbc.E18-09-0549

Nichols, B.J., C. Ungermann, H.R. Pelham, W.T. Wickner, and A. Haas. 1997. Homotypic vacuolar fusion mediated by t- and v-SNAREs. *Nature*. 387: 199–202. https://doi.org/10.1038/387199a0

Novick, P. and R. Schekman. 1979. Secretion and cell-surface growth are blocked in a temperature-sensitive mutant of Saccharomyces cerevisiae. *Proc. Natl. Acad. Sci. USA*. 76:1858–1862. https://doi.org/10.1073/pnas.76.4.1858

Ossig, R., C. Dascher, H.H. Trepte, H.D. Schmitt, and D. Gallwitz. 1991. The yeast SLY gene products, suppressors of defects in the essential GTP-binding Ypt1 protein, may act in endoplasmic reticulum-to-Golgi transport. *Mol. Cell. Biol.* 11:2980–2993. https://doi.org/10.1128/mcb.11.6.2980-2993.1991

Parisotto, D., M. Pfau, A. Scheutzow, K. Wild, M.P. Mayer, J. Malsam, I. Sinning, and T.H. Söllner. 2014. An extended helical conformation in domain 3a of Munc18-1 provides a template for SNARE (soluble N-ethylmaleimide-sensitive factor attachment protein receptor) complex assembly. *J. Biol. Chem.* 289:9639–9650. https://doi.org/10.1074/jbc.M113.514273

Patterson, J.T. 1932. A new type of mottled-eyed Drosophila due to an unstable translocation. *Genetics*. 17:38–59. https://doi.org/10.1093/genetics/17.1.38

Pei, J., C. Ma, J. Rizo, and N.V. Grishin. 2009. Remote homology between Munc13 MUN domain and vesicle tethering complexes. *J. Mol. Biol.* 391: 509–517. https://doi.org/10.1016/j.jmb.2009.06.054

Peng, R., and D. Gallwitz. 2004. Multiple SNARE interactions of an SM protein: Sed5p/Sly1p binding is dispensable for transport. *EMBO J.* 23: 3939–3949. https://doi.org/10.1038/sj.emboj.7600410

Pevsner, J., S.C. Hsu, and R.H. Scheller. 1994. n-Sec1: a neural-specific syntaxin-binding protein. *Proc. Natl. Acad. Sci. USA*. 91:1445–1449. https://doi.org/10.1073/pnas.91.4.1445

Pfeffer, S.R. 2017. Rab GTPases: Master regulators that establish the secretory and endocytic pathways. *Mol. Biol. Cell*. 28:712–715. https://doi.org/10.1091/mbc.e16-10-0737

Pieren, M., A. Schmidt, and A. Mayer. 2010. The SM protein Vps33 and the t-SNARE H(abc) domain promote fusion pore opening. *Nat. Struct. Mol. Biol.* 17:710–717. https://doi.org/10.1038/nsmb.1809

Prinslow, E.A., K.P. Stepien, Y.Z. Pan, J. Xu, and J. Rizo. 2019. Multiple factors maintain assembled trans-SNARE complexes in the presence of NSF and αSNAP. *Elife*. 8:e38880. https://doi.org/10.7554/eLife.38880

Richmond, J.E., R.M. Weimer, and E.M. Jorgensen. 2001. An open form of syntaxin bypasses the requirement for UNC-13 in vesicle priming. *Nature*. 412:338–341. https://doi.org/10.1038/35085583

Rieder, S.E., and S.D. Emr. 1997. A novel RING finger protein complex essential for a late step in protein transport to the yeast vacuole. *Mol. Biol. Cell*. 8:2307–2327. https://doi.org/10.1091/mbc.8.11.2307

Rizo, J., and T.C. Südhof. 2012. The membrane fusion enigma: SNAREs, Sec1/Munc18 proteins, and their accomplices--guilty as charged? *Annu. Rev. Cell Dev. Biol.* 28:279–308. https://doi.org/10.1146/annurev-cellbio-101011-155818

Schwartz, M.L., D.P. Nickerson, B.T. Lobingier, R.L. Plemel, M. Duan, C.G. Angers, M. Zick, and A.J. Merz. 2017. Sec17 (α-SNAP) and an SM-tethering complex regulate the outcome of SNARE zippering in vitro and in vivo. *Elife*. 6:e27396. https://doi.org/10.7554/eLife.27396

Seals, D.F., G. Eitzen, N. Margolis, W.T. Wickner, and A. Price. 2000. A Ypt/Rab effector complex containing the Sec1 homolog Vps33p is required for homotypic vacuole fusion. *Proc. Natl. Acad. Sci. USA*. 97:9402–9407. https://doi.org/10.1073/pnas.97.17.9402

Song, H., A. Orr, M. Duan, A.J. Merz, and W. Wickner. 2017. Sec17/Sec18 act twice, enhancing membrane fusion and then disassembling cis-SNARE complexes. *Elife*. 6:e26646. https://doi.org/10.7554/eLife.26646

Song, H., and W. Wickner. 2019. Tethering guides fusion-competent trans-SNARE assembly. *Proc. Natl. Acad. Sci. USA*. 116:13952–13957. https://doi.org/10.1073/pnas.1907640116

Stanton, A.E., and F.M. Hughson. 2023. The machinery of vesicle fusion. *Curr. Opin. Cell Biol.* 83:102191. https://doi.org/10.1016/j.ceb.2023.102191

Stenmark, H. 2012. The Rabs: A family at the root of metazoan evolution. *BMC Biol.* 10:68. https://doi.org/10.1186/1741-7007-10-68

Stepien, K.P., E.A. Prinslow, and J. Rizo. 2019. Munc18-1 is crucial to overcome the inhibition of synaptic vesicle fusion by αSNAP. *Nat. Commun.* 10:4326. https://doi.org/10.1038/s41467-019-12188-4

Stepien, K.P., J. Xu, X. Zhang, X.C. Bai, and J. Rizo. 2022. SNARE assembly enlightened by cryo-EM structures of a synaptobrevin-Munc18-1-syntaxin-1 complex. *Sci. Adv.* 8:eabo5272. https://doi.org/10.1126/sciadv.abo5272

Struthers, M.S., S.G. Shanks, C. MacDonald, L.N. Carpp, A.M. Drozdowska, D. Kioumourtzoglou, M.L. Furgason, M. Munson, and N.J. Bryant. 2009. Functional homology of mammalian syntaxin 16 and yeast Tlg2p reveals a conserved regulatory mechanism. *J. Cell Sci.* 122:2292–2299. https://doi.org/10.1242/jcs.046441

Südhof, T.C., and J.E. Rothman. 2009. Membrane fusion: Grappling with SNARE and SM proteins. *Science*. 323:474–477. https://doi.org/10.1126/science.1161748

Sutton, R.B., D. Fasshauer, R. Jahn, and A.T. Brunger. 1998. Crystal structure of a SNARE complex involved in synaptic exocytosis at 2.4 A resolution. *Nature*. 395:347–353. https://doi.org/10.1038/26412

Togneri, J., Y.S. Cheng, M. Munson, F.M. Hughson, and C.M. Carr. 2006. Specific SNARE complex binding mode of the Sec1/Munc-18 protein, Sec1p. *Proc. Natl. Acad. Sci. USA*. 103:17730–17735. https://doi.org/10.1073/pnas.0605448103

Toonen, R.F., and M. Verhage. 2003. Vesicle trafficking: Pleasure and pain from SM genes. *Trends Cell Biol.* 13:177–186. https://doi.org/10.1016/S0962-8924(03)00031-X

Ungar, D., and F.M. Hughson. 2003. SNARE protein structure and function. *Annu. Rev. Cell Dev. Biol.* 19:493–517. https://doi.org/10.1146/annurev.cellbio.19.110701.155609

Wang, S., U.B. Choi, J. Gong, X. Yang, Y. Li, A.L. Wang, X. Yang, A.T. Brunger, and C. Ma. 2017. Conformational change of syntaxin linker region induced by Munc13s initiates SNARE complex formation in synaptic exocytosis. *EMBO J.* 36:816–829. https://doi.org/10.15252/embj.201695775

Wang, Y., I. Dulubova, J. Rizo, and T.C. Südhof. 2001. Functional analysis of conserved structural elements in yeast syntaxin Vam3p. *J. Biol. Chem.* 276:28598–28605. https://doi.org/10.1074/jbc.M101644200

Weber, T., B.V. Zemelman, J.A. McNew, B. Westermann, M. Gmachl, F. Parlati, T.H. Söllner, and J.E. Rothman. 1998. SNAREpins: Minimal machinery for membrane fusion. *Cell*. 92:759–772. https://doi.org/10.1016/S0092-8674(00)81404-X

Xu, H., Y. Jun, J. Thompson, J. Yates, and W. Wickner. 2010. HOPS prevents the disassembly of trans-SNARE complexes by Sec17p/Sec18p during membrane fusion. *EMBO J.* 29:1948–1960. https://doi.org/10.1038/emboj.2010.97

Yamaguchi, T., I. Dulubova, S.W. Min, X. Chen, J. Rizo, and T.C. Südhof. 2002. Sly1 binds to Golgi and ER syntaxins via a conserved N-terminal peptide motif. *Dev. Cell*. 2:295–305. https://doi.org/10.1016/S1534-5807(02)00125-9

Yang, B., M. Steegmaier, L.C. Gonzalez Jr., and R.H. Scheller. 2000. nSec1 binds a closed conformation of syntaxin1A. *J. Cell Biol.* 148:247–252. https://doi.org/10.1083/jcb.148.2.247

Yang, J., H. Jin, Y. Liu, Y. Guo, and Y. Zhang. 2022. A dynamic template complex mediates Munc18-chaperoned SNARE assembly. *Proc. Natl. Acad. Sci. USA*. 119:e2215124119. https://doi.org/10.1073/pnas.2215124119

Yang, X., S. Wang, Y. Sheng, M. Zhang, W. Zou, L. Wu, L. Kang, J. Rizo, R. Zhang, T. Xu, and C. Ma. 2015. Syntaxin opening by the MUN domain underlies the function of Munc13 in synaptic-vesicle priming. *Nat. Struct. Mol. Biol.* 22:547–554. https://doi.org/10.1038/nsmb.3038

Yoon, T.Y., and M. Munson. 2018. SNARE complex assembly and disassembly. *Curr. Biol.* 28:R397–R401. https://doi.org/10.1016/j.cub.2018.01.005

Yu, H., S.S. Rathore, C. Shen, Y. Liu, Y. Ouyang, M.H. Stowell, and J. Shen. 2015. Reconstituting intracellular vesicle fusion reactions: The essential role of macromolecular crowding. *J. Am. Chem. Soc.* 137:12873–12883. https://doi.org/10.1021/jacs.5b08306

Zorman, S., A.A. Rebane, L. Ma, G. Yang, M.A. Molski, J. Coleman, F. Pincet, J.E. Rothman, and Y. Zhang. 2014. Common intermediates and kinetics, but different energetics, in the assembly of SNARE proteins. *Elife*. 3:e03348. https://doi.org/10.7554/eLife.03348

Zucchi, P.C., and M. Zick. 2011. Membrane fusion catalyzed by a Rab, SNAREs, and SNARE chaperones is accompanied by enhanced permeability to small molecules and by lysis. *Mol. Biol. Cell*. 22:4635–4646. https://doi.org/10.1091/mbc.e11-08-0680

Supplemental material

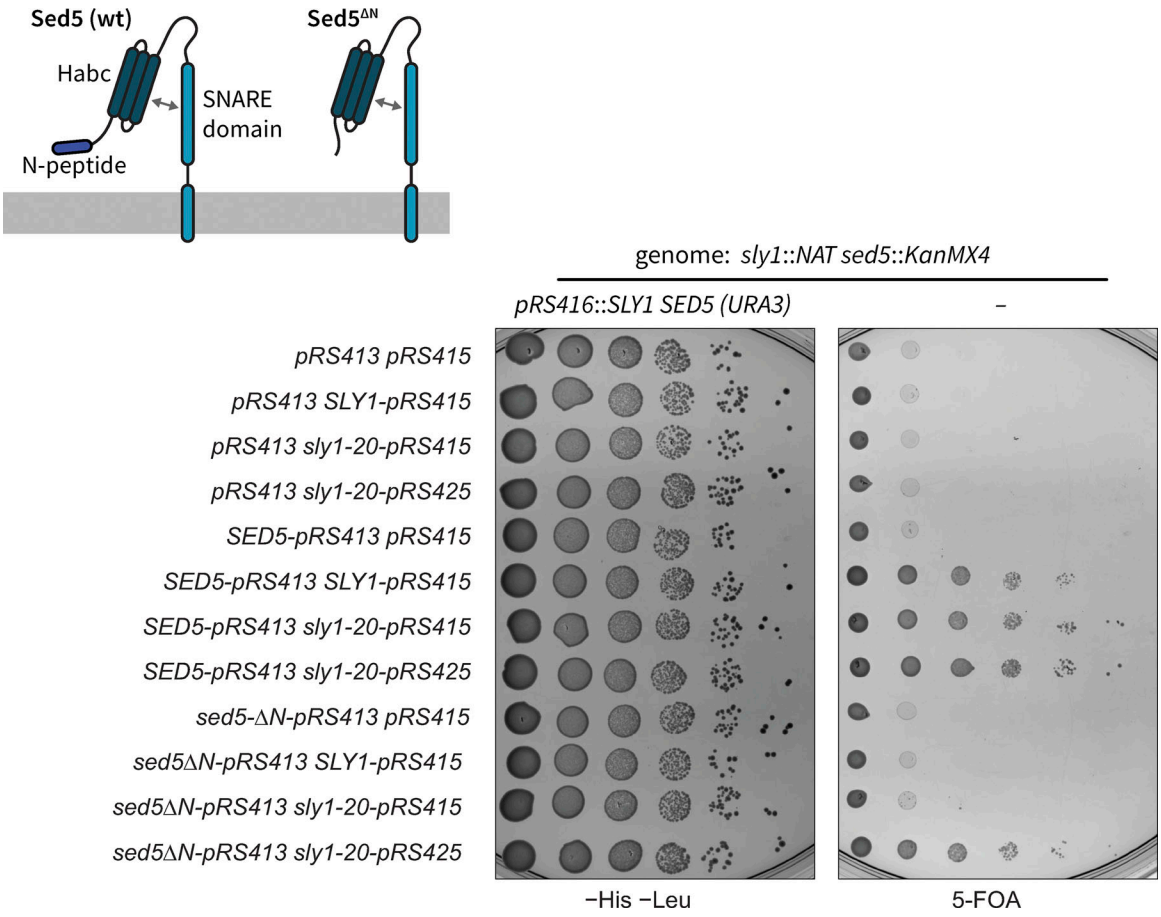

Figure S1. **Genetic interactions among sed5-ΔN, SLY1, and SLY1-20.** This figure shows the results from Fig. 1 B and Fig. 3 A together, along with additional controls. The sed5-ΔN allele was tested using sed5Δ sly1Δ double knockout cells that carry intact copies of both SED5 and SLY1 on a single counter-selectable plasmid. Forced ejection of the SED5 SLY1 plasmid by plating onto 5-fluoroorotic acid (5-FOA) resulted in lethality unless both SED5 and SLY1 (or SLY1-20) were supplied in trans.

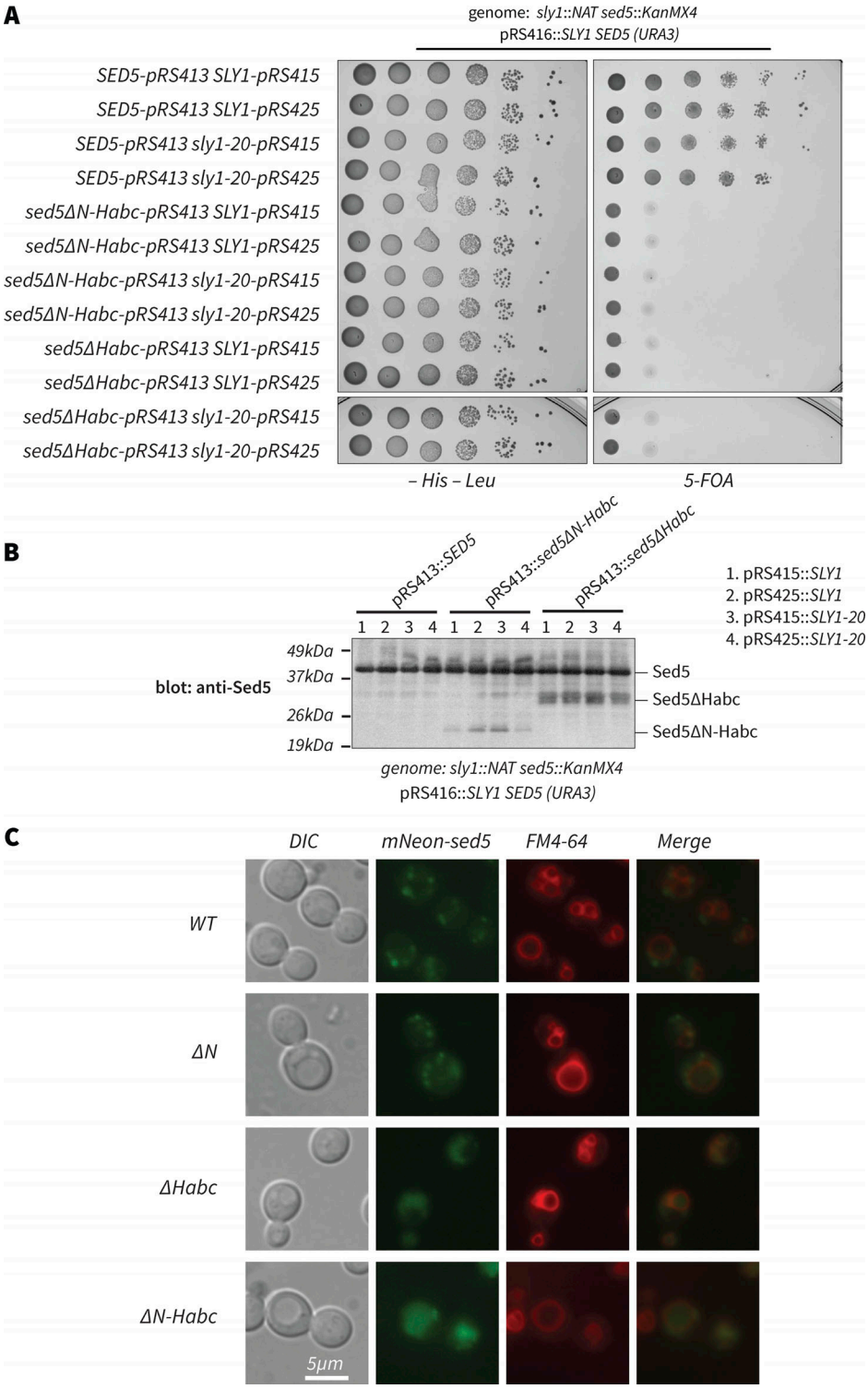

Figure S2. **The Sed5 Habc domain is essential in vivo and necessary for correct Sed5 localization. (A)** sed5 alleles encoding variants lacking the Habc domain do not support viability, even in the presence of high-copy SLY1-20. **(B)** In cells expressing wild-type Sed5, Sed5ΔHabc, and Sed5ΔN-Habc variants are produced in vivo and migrate at the expected sizes. The strains shown in A were grown in –His –Leu media. Whole-cell lysates were prepared, fractionated on SDS-PAGE, and analyzed by immunoblot with anti-Sed5. Note that the anti-Sed5 antibody is polyclonal. Consequently, band intensities for a given Sed5 variant can be used to infer relative abundance. However, the band intensities cannot be used to infer the relative abundance of different Sed5 constructs. **(C)** Subcellular localization of Sed5* variants. Cells expressing both wild-type Sed5 and the indicated mNeon-Sed5* variants were labeled with the vital dye FM4-64 (which marks the vacuolar lysosome), and then examined using Nomarski differential interference contrast (DIC) and epifluorescence. Wild-type Sed5 and Sed5ΔN exhibited a punctate localization not overlapping with FM4-64. This is consistent with Golgi localization at a steady state. In contrast, Sed5ΔHabc and Sed5ΔN-Habc colocalized with FM4-64, consistent with a prevacuolar or vacuolar localization, and appeared to be in the vacuole lumen rather than on the vacuole limiting membrane. Source data are available for this figure: SourceData FS2.

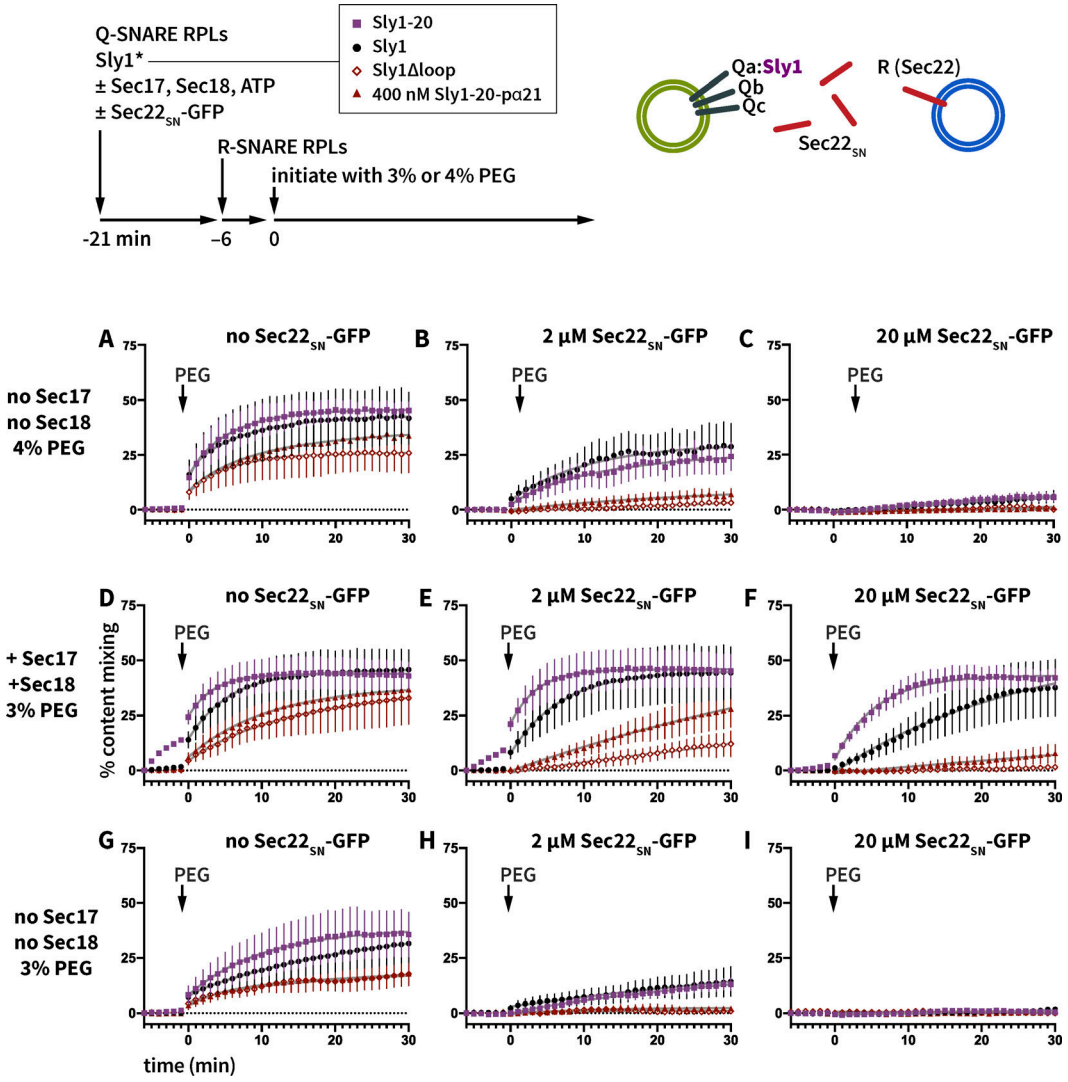

Figure S3. **Helix α21 promotes the selective formation of fusion-active trans-SNARE complexes.** This figure shows additional variations and controls for the experiment shown in Fig. 6. **(A–C and G–I)** In A–C and G–I, Sec17 and Sec18 were omitted, so fusion-dead cis-SNARE complexes were not dynamically recycled. In D–I, PEG was added to 3% rather than 4%. At *t* = −21 min, Q-SNARE RPLs bearing Sed5-WT were mixed with 100 nM SLY1 variants as indicated in the legend, and either with (D–F) or without (A–C and G–I) Sec17, Sec18 (100 nM each), and Mg·ATP (1 mM). Soluble Sec22SN-GFP was added to 0 µM (A, D, and G), 2 µM (B, E, and H), or 20 µM (C, F, and I). At *t* = −6 min R-SNARE RPLs were added. At *t* = 0, fusion was initiated by the addition of PEG. Points show mean ± SEM of at least three independent experiments. Gray lines show least-squares fits of a second-order kinetic function.

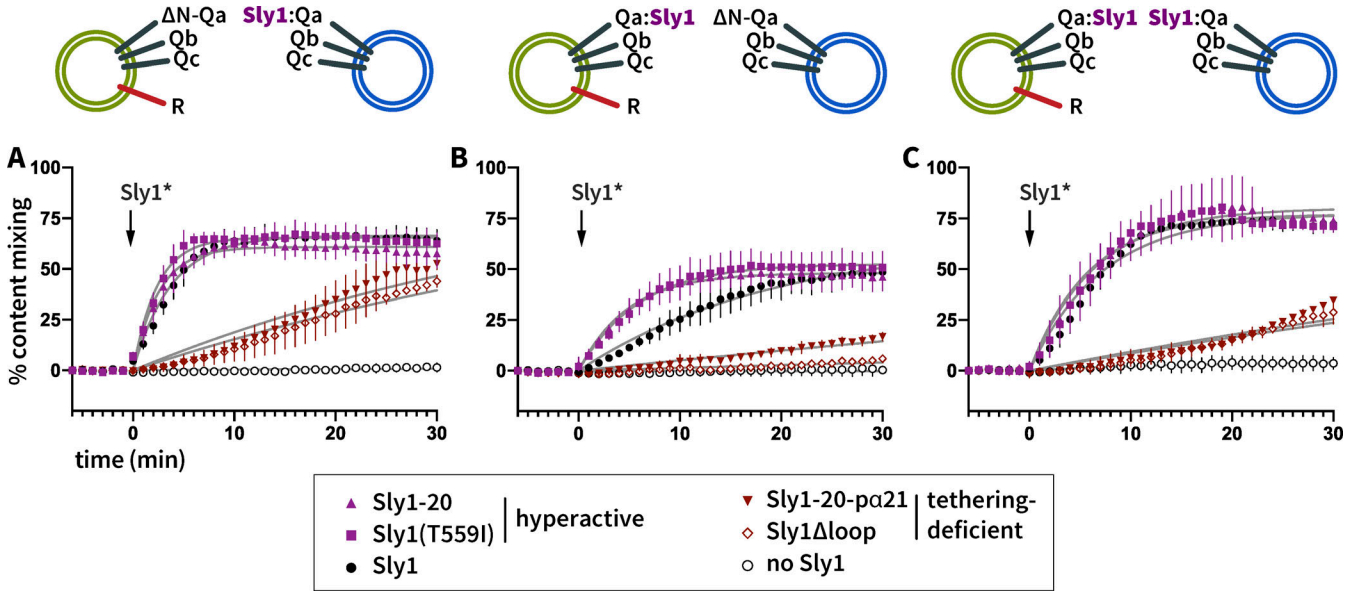

Figure S4. **Helix α21 promotes the selective formation of fusion-active trans-SNARE complexes.** This experiment is identical to the one shown in Fig. 7, except that 1,600 nM Sly1 or Sly1 variants were present in the reactions rather than 100 nM.

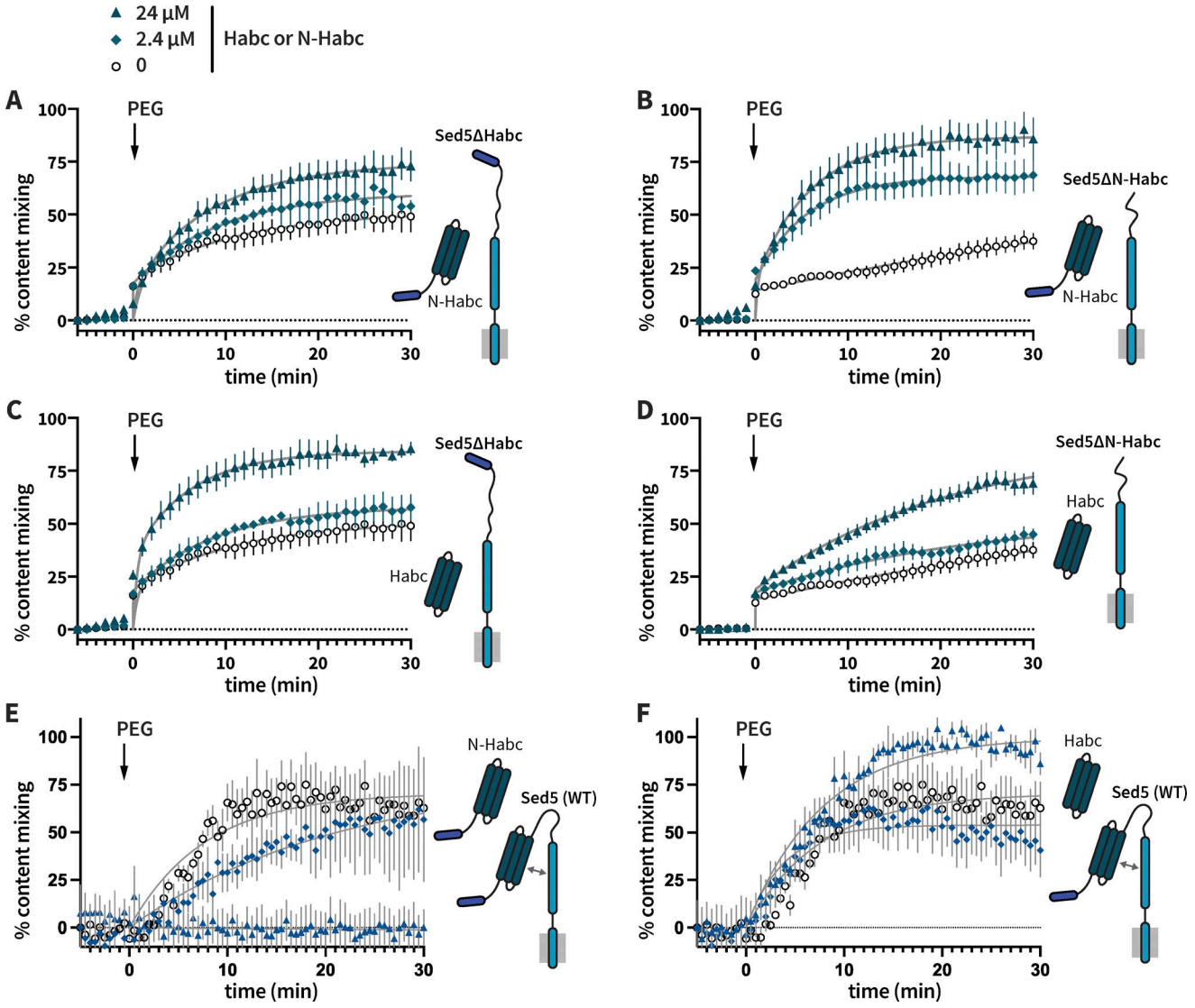

Figure S5. **Soluble Sed5 Habc domain can stimulate Sly1-dependent fusion in the absence of Sec17 and Sec18.** These experiments are like the ones in Fig. 8, except that Sec17 and Sec18 were omitted. **(A–F)** At t = −6 min, R-SNARE RPLs and Q-SNARE RPLS were mixed with 1.5 µM Sly1 that had been preincubated with either soluble Sed5N-Habc (A, B, and E) or Sed5Habc (C, D, and F). At t = 0, the reactions were initiated by the addition of 3% PEG. Points show mean ± SEM of at least three independent experiments. Gray lines show least-squares fits of a second-order kinetic function. The experiments in A–C were done in parallel with the experiments in Fig. 8 and separately from the experiments in E and F.

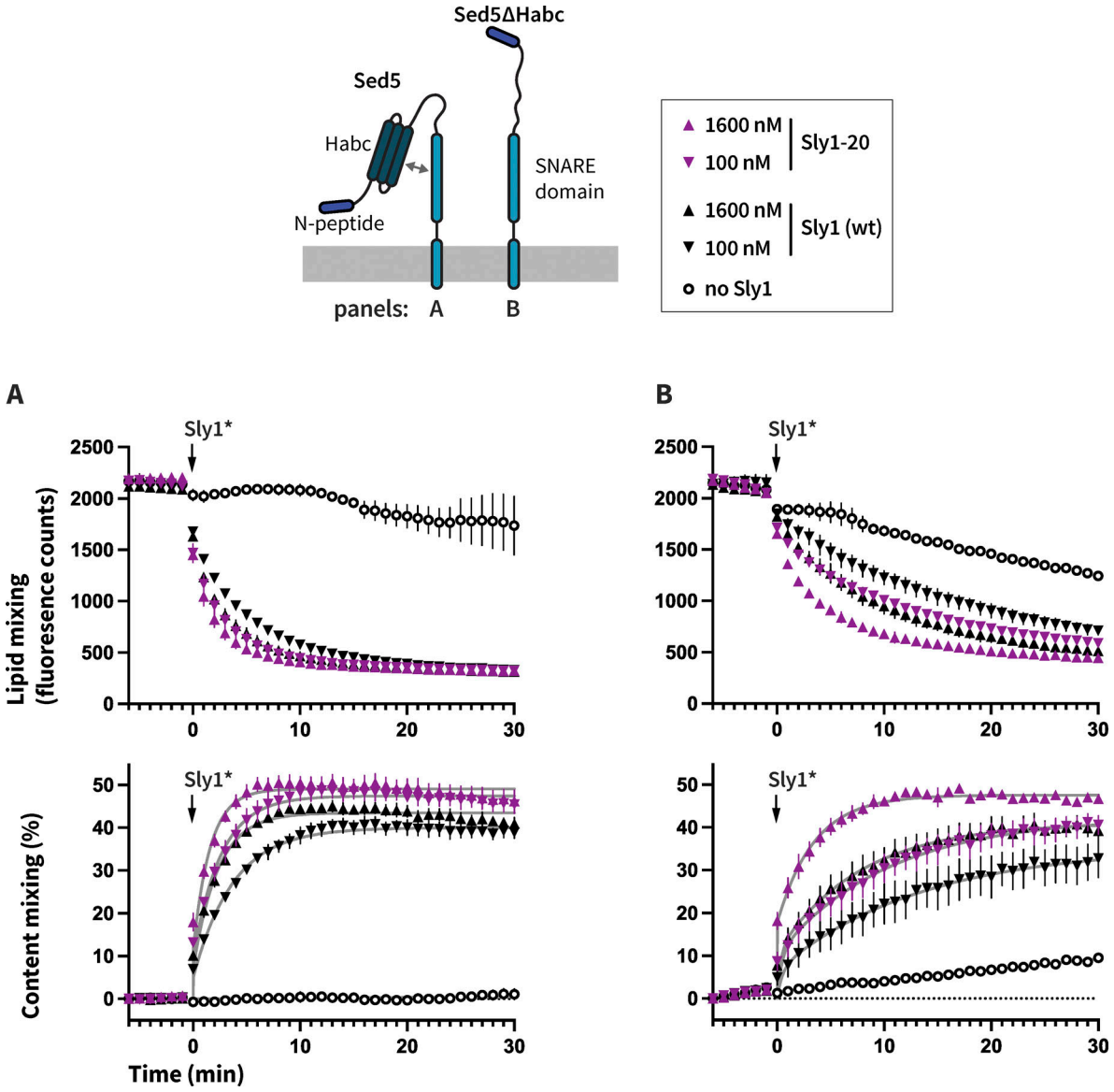

Figure S6. **Effects of Sed5 Habc domain deletion on lipid and content mixing.** Parallel lipid (top) and content mixing (bottom) results are shown from the same sets of reactions. **(A and B)** The content mixing data in A and B are identical to Fig. 4, B and D, and are shown here to facilitate comparison with the lipid mixing data. At t = −6 min, reactions were initiated with RPLs indicated in the cartoon, in the presence of 3% PEG, 100 nM Sec17, 100 nM Sec18, and 1 mM Mg·ATP. At t = 0, Sly1 or Sly1-20 was added to the reactions at 0, 100, or 1,600 nM, as indicated in the legend in the upper right corner. Lipid mixing is reported as raw fluorescence counts in arbitrary units. As the membranes mix, FRET from Marina Blue DHPE to NBD-DHPE (initially in separate liposomes) quenches Marina Blue emission at 465 nm. Points show mean ± SEM of at least three independent experiments. Gray lines show least-squares fits of a second-order kinetic function.

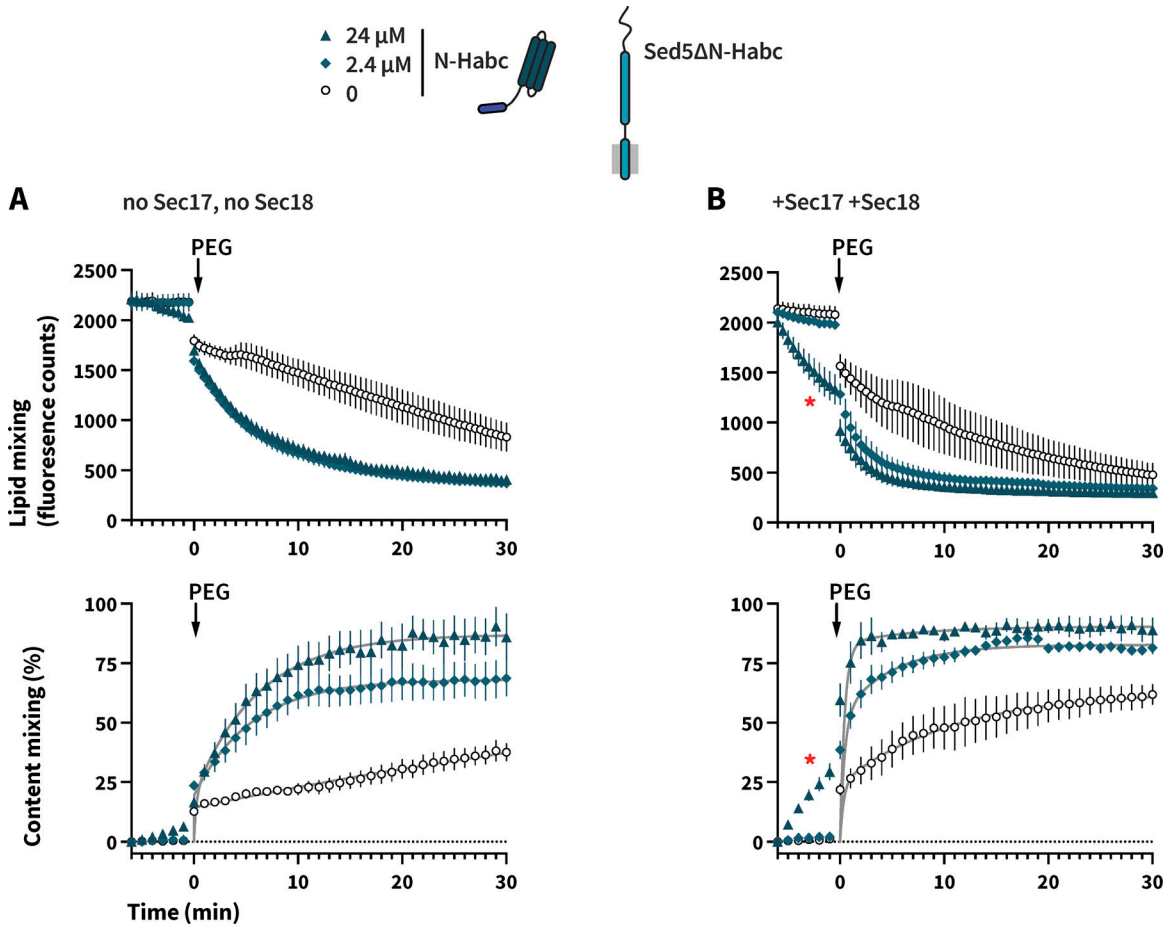

Figure S7. **Effects of soluble Habc domain on lipid and content mixing.** Parallel lipid (top) and content mixing (bottom) results are shown from the same sets of reactions. **(A and B)** The content mixing data in A and B are identical to Fig. 8 B and Fig. S5 B and are shown here to facilitate comparison with the lipid mixing data. At t = −6 min, R-SNARE RPLs and Q-SNARE RPLS were mixed with 1.5 µM Sly1 that had been preincubated with or without soluble Sed5N-Habc. Sec17 and Sec18 were absent (A) or added to 100 nM (B). At t = 0, the reactions were initiated by the addition of 3% PEG. Lipid mixing is reported as raw fluorescence counts in arbitrary units. As the membranes mix, FRET from Marina Blue DHPE to NBD-DHPE (initially in separate liposomes) quenches Marina Blue emission at 465 nm. Red asterisks (*) indicate Habc-dependent lipid and content mixing occurring prior to the addition of PEG. Points and bars show means ± SEM of data from three separate experiments.

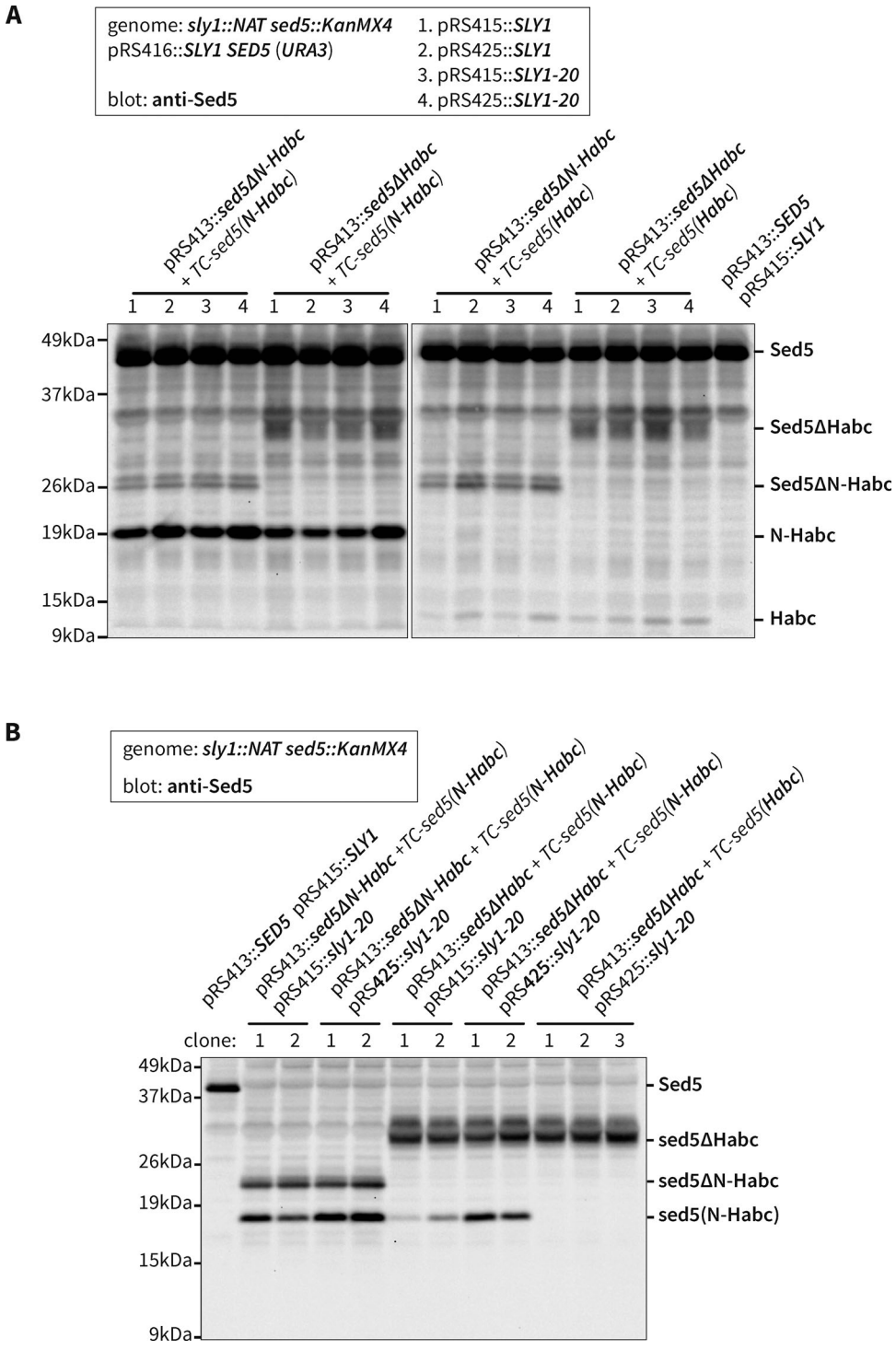

Figure S8. **Coexpression of mutant Sed5 proteins and N-terminal Sed5 fragments.** Whole-cell lysates from the indicated strains were prepared, separated by SDS-PAGE, and immunoblotted with anti-Sed5. A shows expression in strains containing a counter-selectable SLY1 SED5 balancer plasmid. Panel B shows expression in strains harboring SLY1-20 on single-copy (pRS415) or multicopy (pRS425) plasmids following the ejection of the SLY1 SED5 balancer plasmid. Source data are available for this figure: SourceData FS8.

Provided online is Table S1. Table S1 shows the yeast strains and plasmids used in this study.